Dr-610
ORNL-5240
UC-25

Study of Iridium and Iridium-Tungsten Alloys for Space Radioisotopic Heat Sources

C. T. Liu
H. Inouye

OAK RIDGE NATIONAL LABORATORY
OPERATED BY UNION CARBIDE CORPORATION FOR THE ENERGY RESEARCH AND DEVELOPMENT ADMINISTRATION

DISCLAIMER

Printed in the United States of America. Available from
National Technical Information Service
U.S. Department of Commerce
5285 Port Royal Road, Springfield, Virginia 22161
Price: Printed Copy $4.50; Microfiche $3.00

ORNL-5240
Distribution
Category

Contract No. W-7405-eng-26

METALS AND CERAMICS DIVISION

STUDY OF IRIDIUM AND IRIDIUM-TUNGSTEN ALLOYS FOR SPACE RADIOISOTOPIC HEAT SOURCES

C. T. Liu
H. Inouye

Date Published: December 1976

OAK RIDGE NATIONAL LABORATORY
Oak Ridge, Tennessee 37830
operated by
UNION CARBIDE CORPORATION
for the
ENERGY RESEARCH AND DEVELOPMENT ADMINISTRATION

CONTENTS

STUDY OF IRIDIUM AND IRIDIUM-TUNGSTEN ALLOYS FOR SPACE RADIOISOTOPIC HEAT SOURCES

C. T. Liu and H. Inouye

ABSTRACT

The physical and mechanical properties of iridium and iridium-tungsten alloys containing up to 4% tungsten have been evaluated as potential cladding materials in space isotopic heat sources. The iridium-tungsten alloys are readily fabricable and are compatible with graphite, low-pressure oxygen, and simulated heat source environments up to at least 1300°C. The solubility of oxygen and carbon in the alloys appears to be quite low — at a level of 5 ppm for oxygen and 10 ppm for carbon up to 1300°C. The Ir-2% W has good oxidation resistance below 1000°C. No internal oxidation or grain-boundary penetration has been observed in this alloy. Also, alloying with 2% tungsten raises the recrystallization temperature of iridium by 400°C and retards the grain growth at high temperatures.

Tensile properties of iridium and iridium-tungsten alloys were determined as a function of test temperature up to 1400°C. Alloying with tungsten increases the yield strength and slightly lowers the ductility. The ductilities of the alloys increase steadily with test temperature. In connection with this increase, the fracture mode changes from grain-boundary separation to transgranular fracture at temperatures around 800°C and finally to ductile rupture with close to 100% reduction in area above 1000°C. The Ir-2% W alloy has the best toughness, because of its high strength and good ductility at 1370°C. The yield strength and fracture behavior of iridium and iridium-tungsten alloys were found to be very sensitive to trace impurities with concentrations in the ppm range.

INTRODUCTION

The radioisotopic fuel used for space power systems must be clad in a highly reliable material, not only to contain the fuel for normal operation for several years, but also to survive potential accident conditions such as launchpad abort, aerodynamic heating on reentry, high-velocity impact, and the postimpact environment. Advanced heat sources require fuel-cladding temperatures ranging from 800 to 1400°C. The environment of these heat sources generally consists of helium and/or argon plus low-pressure active gases derived from decomposition of the oxide fuel and from the outgassing of graphite and insulator materials. This environment limits the use of refractory alloys such as niobium- and tantalum-base alloys, which readily pick up the gaseous impurities, resulting in severe degradation of their mechanical properties.[1,2]

The noble metals are currently the only cladding materials capable of meeting the requirements of advanced heat sources. Iridium and its alloys appear suitable for service up to 1400°C, and platinum alloys appear suitable for temperatures between 800 and 1100°C. The alloy Ir-0.3% W is currently used as the fuel-encapsulating material in the multi-hundred-watt (MHW) heat source[3] operating at 1330°C. Iridium was selected as the base material because of its high melting point, oxidation resistance (below 1000°C), and compatibility with PuO_2 fuel and graphite up to 1500°C. Tungsten, at a level of 0.3 wt %, is added in order to increase the recrystallization temperature and improve the sheet fabrication of iridium. A detailed description of the production of Ir-0.3% W sheets and disks for fuel cladding in the MHW heat source has been reported recently by Braski and Schaffhauser.[4]

As a part of a general research and development effort in support of space radioisotopic heat-source programs sponsored by the Division of Nuclear Research and Applications, Energy Research and Development Administration, we have been studying the physical and mechanical properties of iridium-tungsten alloys. The objective of this study was threefold:

(1) To characterize the physical and mechanical properties of iridium in order to obtain a better understanding of the metallurgical factors controlling these properties.
(2) To characterize the Ir-0.3% W sheet material used for the production of MHW postimpact containment shells (PICS) for space flight missions. The properties of Ir-0.3% W alloy are not well characterized from lot to lot.[5] Thus, this study emphasized the determination of lot-to-lot or heat-to-heat variations in properties.
(3) To develop iridium-tungsten alloys with suitable properties for fuel encapsulation in advanced heat sources.

In the present work, iridium alloys containing up to 4% tungsten were prepared and fabricated into 0.05 to 0.08-cm-thick sheets. The test program described below involved the determination of formability, recrystallization and grain-growth behavior, air oxidation, tensile properties, and compatibility with graphite and/or low-pressure oxygen.

ALLOY PREPARATION AND FABRICATION

Alloy Preparation

The starting materials used for preparation of iridium and iridium-tungsten alloys were obtained from different sources, including the U.S. Office of Emergency Preparedness (OEP), Matthey-Bishop (MB) Inc., and Engelhard Industries (EI). The chemistry of these materials (listed in Table 1) was determined by spark-source mass-spectrometric (SSMS) analysis.

OEP Powder

The iridium powder used to prepare the MHW PICS and most of the iridium-tungsten alloys was obtained from OEP in 40- to 60-kg shipments.

Table 1. Chemical analysis[a] of iridium and iridium-tungsten alloys

Element	Starting material					Alloy sheet							
	Ir powder			Ir plate,	W	Ir	Ir-0.3% W		Ir-0.5% W	1% W	2% W		4% W
	MB[b]	WC[c]	WG[c]	S-74[d]	powder	EB[e]	WC	WG	Ir-33	Ir-19	Ir-15	Ir-38, Ir-39	Ir-29
						SSMS[f]-analysis							
Al	4	1	0.5	70	4	2	2	5	3	1	3	1	2
B	0.5	0.6	0.1	1.4		0.1	0.2	0.5	1	0.2	<1	0.2	1
Ca	20	60	5	30		2	6		0.1	2	6	6	0.1
Co	0.3	0.1	0.3	2		0.1	6	0.1	0.1	0.1	1	6	0.1
Cr	0.8	1	2	100	20	3	30	5	2	10	3	3	2.0
Cu	4	2	3	30	8	5	3	1	0.3	1	1	3	0.3
Fe	8	10	5	400		10		5	3	15	10	15	20
Hf							<0.4			4		<0.4	
K	20	20	5	<0.6		0.2	6	3	3	2	6	6	3
Mg	3	10	1	5	2	0.4	0.4	1	0.3	<0.4	<1	<0.4	0.3
Mn	0.8	1	1	3	2	0.1	0.3	0.1	0.1	0.3	1	0.3	0.1
Mo		<3	0.3	3	30	20	3	10	1	3	20	10	10
Ni	0.3	2	1.5	50		0.1	1	1	0.3	1	1	1	3
Os		0.4					<0.4			<0.4		<0.4	
P	0.1	0.5	0.1	0.3		0.1	0.3	0.1	0.1	0.1	1	0.1	0.5
Pd	60	2	1	20		0.2	<0.2			<0.2		<0.2	
Pt		10		100		1	1		30	1		1	40
Re		<0.5		<0.5	50		<0.2			<0.2	3	6	
Rh	15	80	50	150		15	2	20	2	20	1	2	5
Rn		15	3	150			20	20	7	200	50	20	7
Si	8	30	10	60	6	3	100	5	10	3	30	30	30
Sn					10	0.2	<0.2			<0.2		<0.2	
Ta	0.8	<3	1	10		30	3	10	10	100	30	3	30
Th				10	100	10	<0.1			1	1	<0.1	
Ti		2		⩽5			⩽3		5	3	15	⩽3	5
V		1	0.1	3	20	1	3	3	0.3	10	1	3	1
W		0.3		∿3000	M	100	4000	3000	∿5000	∿10,000	>10,000	>10,000	>20,000
Zn		3	1				0.1		<0.1	0.1	1	0.1	<0.1
Zr			0.1	1	20		0.3	5	0.3	0.3	300	1	1
Br		3					<0.1			<0.1	10	<0.1	
S	10	10	5	7	20	4	1			3	15	1	
Cl		30	20				8			3	6	5	
						Carbon and vacuum fusion analysis							
O				10			5		3		8	9	2
N				1			1		1		1	2	1
H				1			1		<1		1	1	<1
C				5			9		5		11	8	18

[a] In parts per million by weight.

[b] Matthey Bishop, Inc.

[c] WC and WG are designations of iridium powder shipments of the U.S. Office of Emergency Preparedness. The second letter refers to the sequence of the shipment.

[d] S-74 — an Ir-0.3% W plate supplied by Englehard Industries.

[e] EB — designation for the iridium sheets prepared from Matthey Bishop iridium powder.

[f] Spark-source mass-spectrometric analysis.

Each shipment of powder was designated as WA, WB, WC, etc., where the consecutive alphabetic letters refer to the sequence of the shipment of iridium powder. The chemistry of WC and WG powders as listed in Table 1 shows no major difference between them. The OEP powders are quite pure; their total impurities are around 300 ppm by weight after a washing treatment.[4]

MB Powder

The chemistry of the iridium powder purchased from Matthey Bishop, Inc., is also listed in Table 1. The MB powder is relatively pure and contains a total of about 200 ppm trace impurities. Iridium sheets prepared from this powder are designated EB.

EI Material

The 0.051-cm-thick iridium sheet (S-69) and 0.32-cm-thick iridium (S-65) and Ir-0.3% W (S-74) plates were purchased from Engelhard Industries. The EI material contains much higher levels of impurities, as shown in Table 1. The Ir-0.96% W (Ir-19) and IR-1.92% W (Ir-15) alloys were prepared from the EI material S-74.

Melting and Casting

Tungsten in powder form (with chemistry also in Table 1) was used to prepare iridium-tungsten alloys for improving its dissolution and minimizing its segregation. The tungsten powder was blended thoroughly with the iridium powder and cold-pressed into 70 to 150-g rectangular compacts. The pressed compacts were sintered in hydrogen at 1000°C for 1 hr and in a vacuum at 1500°C for 4 hr. The sintered iridium-tungsten compacts were then electron-beam-melted several times and cast into rectangular-shaped buttons with dimensions of 0.8 x 2.5 x 5.1 cm (Fig. 1*a*) or drop cast[4] into rectangular-cross-section ingots 1.91 x 1.91 x 5.40 cm (Fig. 2). The 150-g alloy buttons were used for initial alloy development studies, and the 400-g ingots were used for the scale-up study. Table 2 lists the composition and preparation of the alloys studied. The heat designated EBP-19 was originally prepared from pure iridium powder, however, its sintered compacts picked up 0.09% tungsten during heat treatment in a tungsten-mesh furnace under poor vacuum conditions (10^{-2} Pa). The Ir-0.3% W sheets are the current PICS material for the MHW heat source; their detailed preparation and fabrication have been reported by Braski and Schaffhauser.[4] The alloys containing up to 4% W were processed into sheets. Alloys with more than 4% W were not processed because of their poor oxidation resistance and tensile ductility.

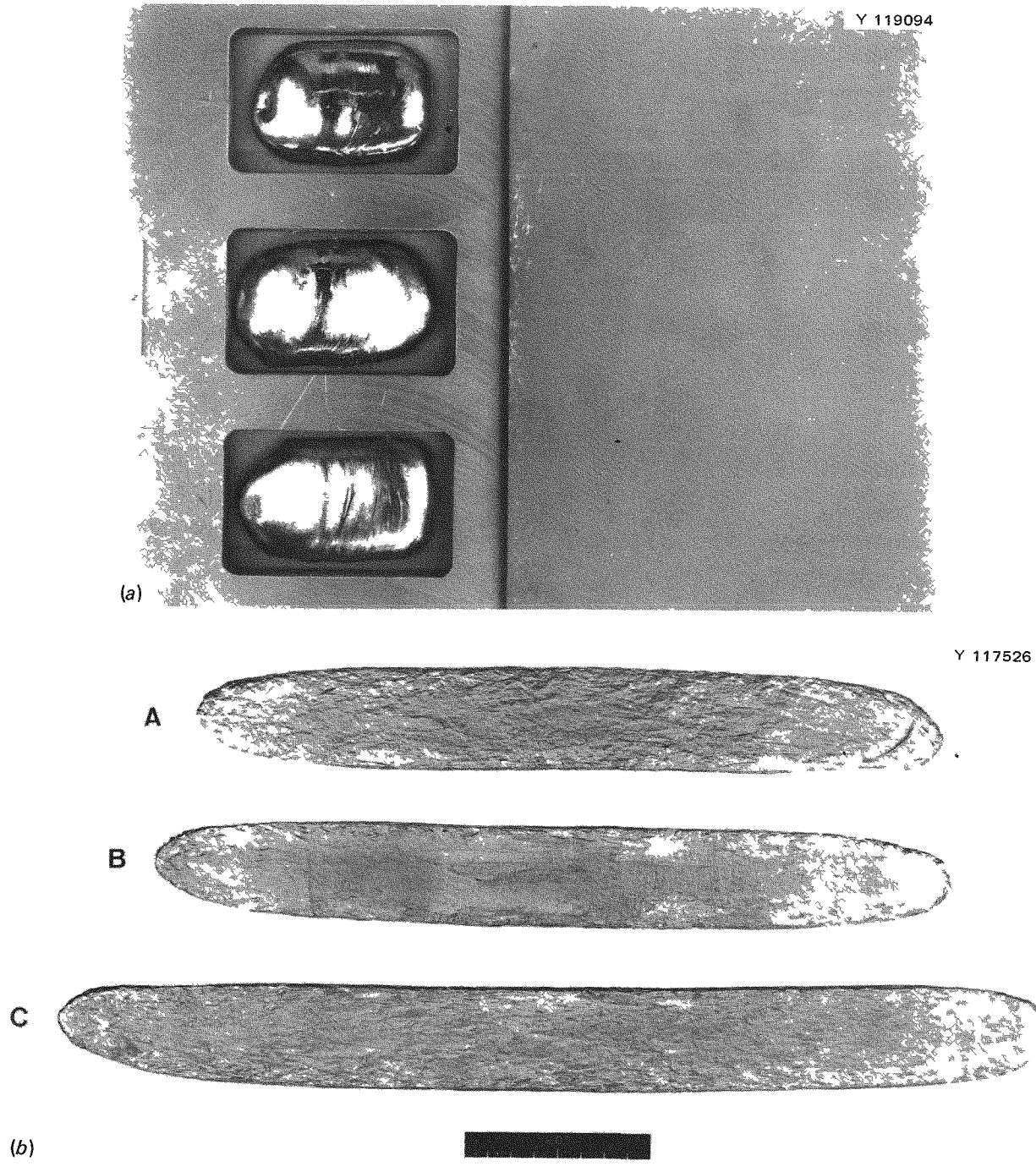

Fig. 1. Iridium-tungsten alloy buttons and plates. (*a*) Alloy buttons clad in molybdenum frame. (*b*) Alloy plates after 65% breakdown rolling at 1200 to 1300°C; A, Ir-1.92% W; B, Ir-0.5% W; C, Ir-0.1% W.

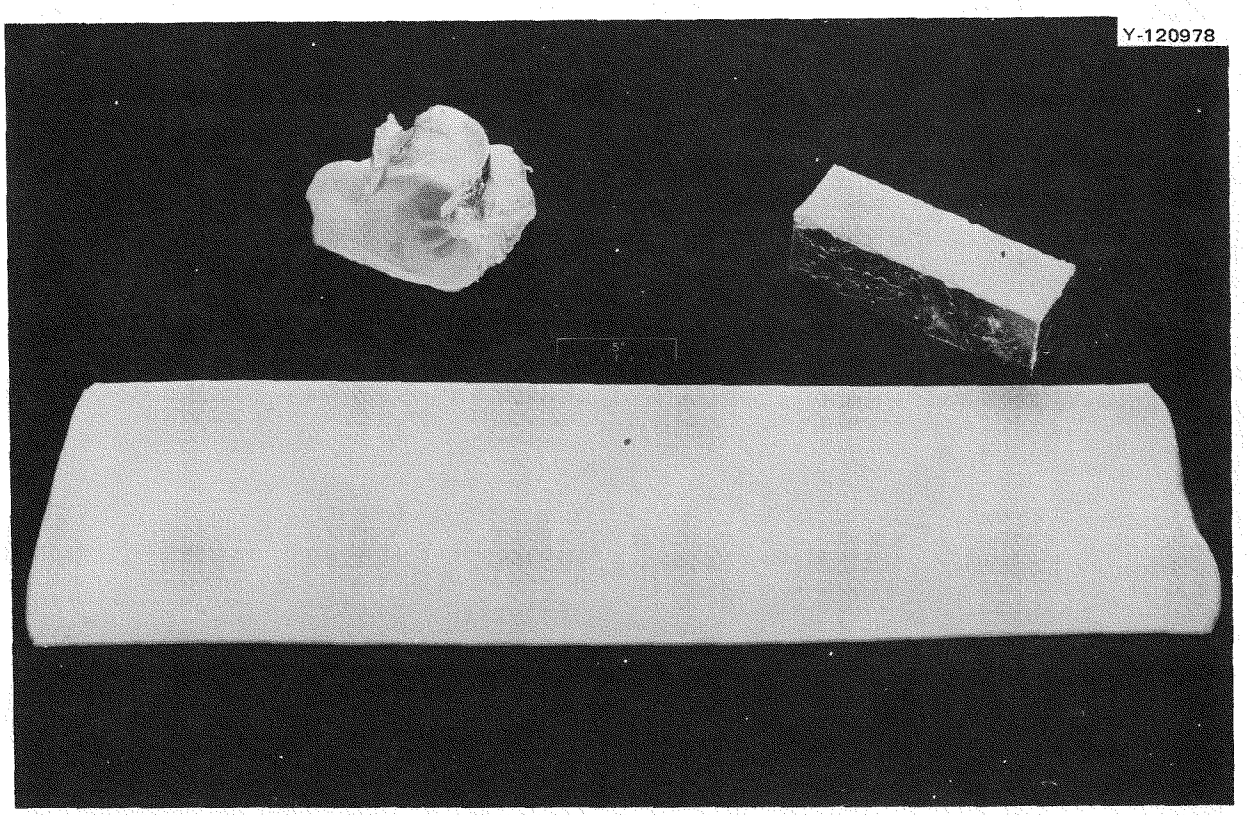

Fig. 2. Electron-beam-melted and drop-cast Ir-1.92% W alloy ingot and head, and fabricated sheet.

Sheet Fabrication

The as-cast alloy buttons or ingots were first cleaned in a solution of aqua regia plus 15% HF solution for about 30 min and were next clad in molybdenum jackets and sealed by electron beam welding. The assemblies were then rolled between 1200 and 1300°C under a partial argon atmosphere with 10 to 15% reduction per pass and an 8- to 10-min reheating period. Hot rolling was stopped after 65% reduction, and the plates (about 0.25 cm thick) were cleaned electrolytically in KCN solution. Figure 1 shows the alloy buttons clad in the molybdenum frame and shows the alloy plates after breakdown rolling. The alloy plates exhibited a lumpy surface characteristic of a highly deformed grain structure, but no edge or surface cracks were observed.

After breakdown rolling, the alloy plates were recrystallized in a vacuum between 1200 and 1400°C for 1 hr. The recrystallized plates were wrapped in a loose-fitting molybdenum cover sheet and rolled to 0.6- to 0.8-mm-thick sheets between 900 and 1100°C. The higher rolling and heat-treatment temperatures were used for the alloys containing higher tungsten contents. The finished iridium-tungsten sheets were removed from the molybdenum cover sheet and again cleaned electrolytically. The finished sheets generally exhibited some minor edge cracks, their number and degree increasing with tungsten contents above 2%. Figure 2 shows the good quality of Ir-1.92% W sheet fabricated from a drop-cast ingot.

Table 2. Alloy composition and preparation

Alloy composition (wt %)	Heat or lot number	Starting iridium material	Alloy preparation		Ingot	
			Melting	Casting	Wt (g)	Size (cm)
Ir	EBP-21	WA powder	EB[a]	Drop	400	1.91 x 1.91 x 5.4
Ir	EB	MB powder	EB	Drop	320	1.91 x 1.91 x 5.4
Ir-0.09 W	EBP-19	WA powder	EB	Drop	400	1.91 x 1.91 x 5.4
Ir-0.1 W	Ir-32	WC powder	EB	Regular	150	∿0.8 x 2.5 x 5.1
Ir-0.3 W	WC, NCR	WC powder	EB	Drop	400	1.91 x 1.91 x 5.4
	WD	WD powder	EB	Drop	400	1.91 x 1.91 x 5.4
	WE, WCR	WE powder	EB	Drop	400	1.91 x 1.91 x 5.4
	WG	WG powder	EB	Drop	400	1.91 x 1.91 x 5.4
Ir-0.5 W	Ir-33	WC powder	EB	Regular	150	∿0.8 x 2.5 x 5.1
Ir-0.96 W	Ir-19	S-74 plate	EB	Regular	150	∿0.8 x 2.5 x 5.1
Ir-1.92 W	Ir-15	S-74 plate	EB	Regular	150	∿0.8 x 2.5 x 5.1
	Ir-38, 39	WC powder	EB	Drop	400	1.91 x 1.91 x 5.4
Ir-3.84 W	Ir-29	WC powder	EB	Drop	150	∿0.8 x 2.5 x 5.1

[a]Electron beam.

The iridium-tungsten alloy sheets were chemically analyzed by various methods after being recrystallized at 1500°C for 1 hr. Atomic absorption analysis indicated that sheets Ir-15 and -39 contained 1.91% tungsten, which is very close to the nominal content of 1.92% W. The SSMS analysis in Table 1 shows that the total trace impurities in alloy sheets are lower than those in their starting materials, indicating purification of iridium by electron-beam melting. The impurity content in the alloy sheets prepared from OEP and MB iridium powders is distinctly lower than that in the sheets produced from the EI material. The interstitial content in these electron-beam-melted alloys is quite low, as shown in Table 1. The oxygen and carbon contents are less than 10 and 20 ppm, respectively, and the hydrogen and nitrogen contents are negligible.

Forming

The Ir-1.92% W sheets produced from drop-cast ingots Ir-38 and -39 were fabricated into hemispheres and capsule assemblies to demonstrate the fabricability of iridium-tungsten alloys. Four disks were cut from the sheets by Elox electrical discharge machining and ground to the final dimensions, 6.03 cm in diameter by 0.0645 cm thick (Fig. 3). Dye penetration and ultrasonic inspection of the disks showed no areas of nonbond, such as laminations or porosities. The disks were heat treated for 1 hr at 1150°C and formed successfully at 800°C at Mound Laboratory.[6]

A part of the alloy sheet was further rolled from 0.081 to 0.058 cm thick for capsule fabrication. Rectangular blanks were cut from the sheet stock and formed over a mandrel to right circular cylinders. The blanks cracked during cold-forming but formed readily over the mandrel when heated with a torch in the range of 600 to 800°C. The warm-formed cylinders were then electron-beam-welded and ground to final dimensions, 1.407 cm outside diameter by 2.159 cm long by 0.0381 cm thick. Disks and end lids were stamped directly from the sheet stock. The four complete sets of capsules delivered to Donald W. Douglas Laboratory are shown in Fig. 4.

MICROSTRUCTURE, RECRYSTALLIZATION, AND GRAIN-GROWTH BEHAVIOR

The iridium-tungsten sheets produced by warm rolling between 900 and 1100°C had essentially a fibrous structure (Fig. 5). A few small recrystallized grains were occasionally observed in iridium containing less than 0.3% W. The sheet specimens of iridium-tungsten alloys were heat treated in vacuum for 1 hr at temperatures between 700 and 1600°C to study their recrystallization and grain-growth behavior. The recrystallization temperatures (T_R) were determined metallographically, and the results were presented in Fig. 6 as a function of tungsten content. Recrystallization of unalloyed iridium (EBP-21) starts at 800°C and is complete at 950°C. The recrystallization temperature increases sharply with tungsten content up to 1% and moderately with tungsten content between 1 and 2%. Alloying with 2% W raises the

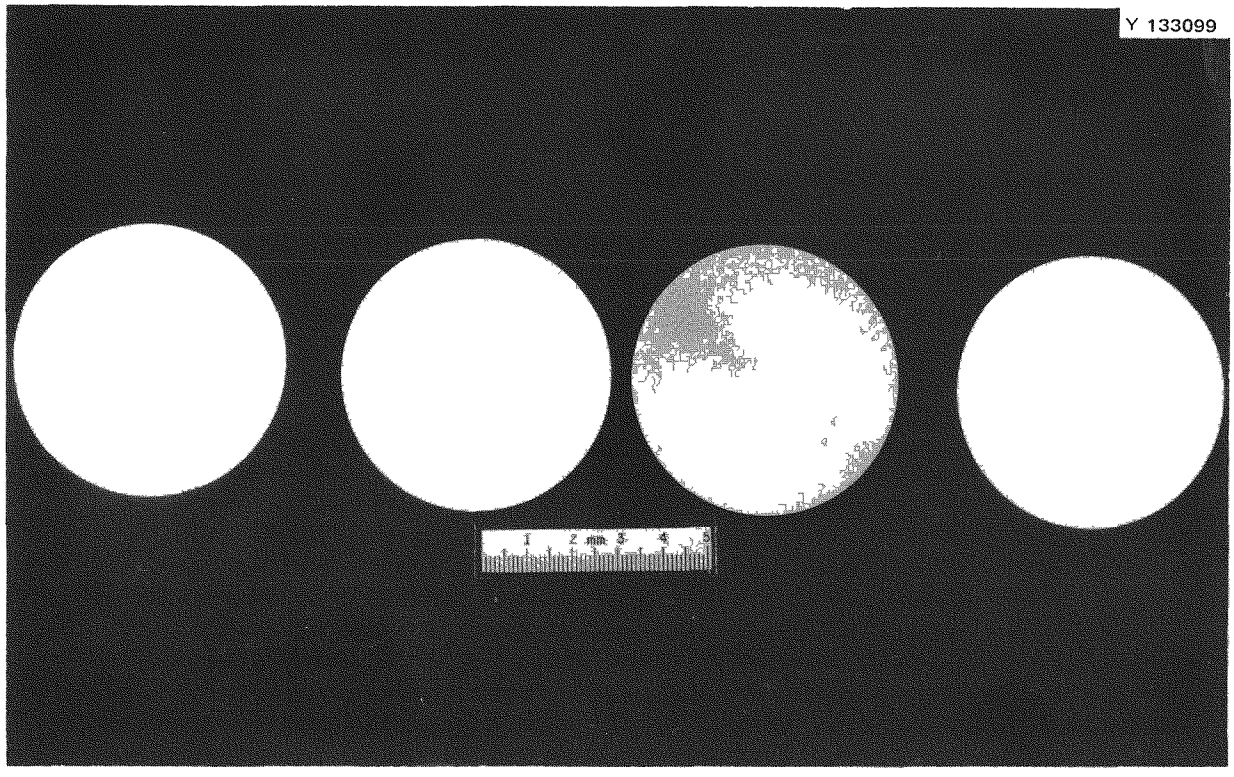

Fig. 3. Four Ir-1.92% W disks with dimensions 0.0645 cm thick x 6.03 cm in diameter.

recrystallization temperature by approximately 400°C. However, no further increase in recrystallization temperature is observed at higher tungsten levels. Figure 5 shows the recrystallized microstructure of the iridium-tungsten alloys. All alloys were single phased, in agreement with the reported[7] phase diagram, which indicates that the maximum of tungsten solubility in iridium is more than 10% below 1000°C. Table 3 summarizes the grain-growth data of the iridium-tungsten alloys. Alloying with 0.3% W or more effectively inhibited grain growth at high temperatures. For example, the grain size, after annealing for 1 hr at 1600°C, was reduced from ASTM grain size 1 to 3-4 when iridium was alloyed with 0.3% W.

As indicated in Fig. 5*c*, annealing at 1500°C for 1 hr produced a uniform grain structure with ASTM grain size No. 4-5 in the Ir-0.3% W sheet WC-4. However, huge grains with ASTM No. 1-2 have been observed frequently in Ir-0.3% W PICS produced from certain lots (for example, lot WE) after a final anneal for 1 hr at 1500°C. The possible causes of the large grains are (1) critical strain induced on forming the blank into a hemisphere, (2) intermediate anneal at 1050 to 1175°C, (3) deformation due to mishandling the hemisphere, and (4) instability of grain boundaries at high temperature.

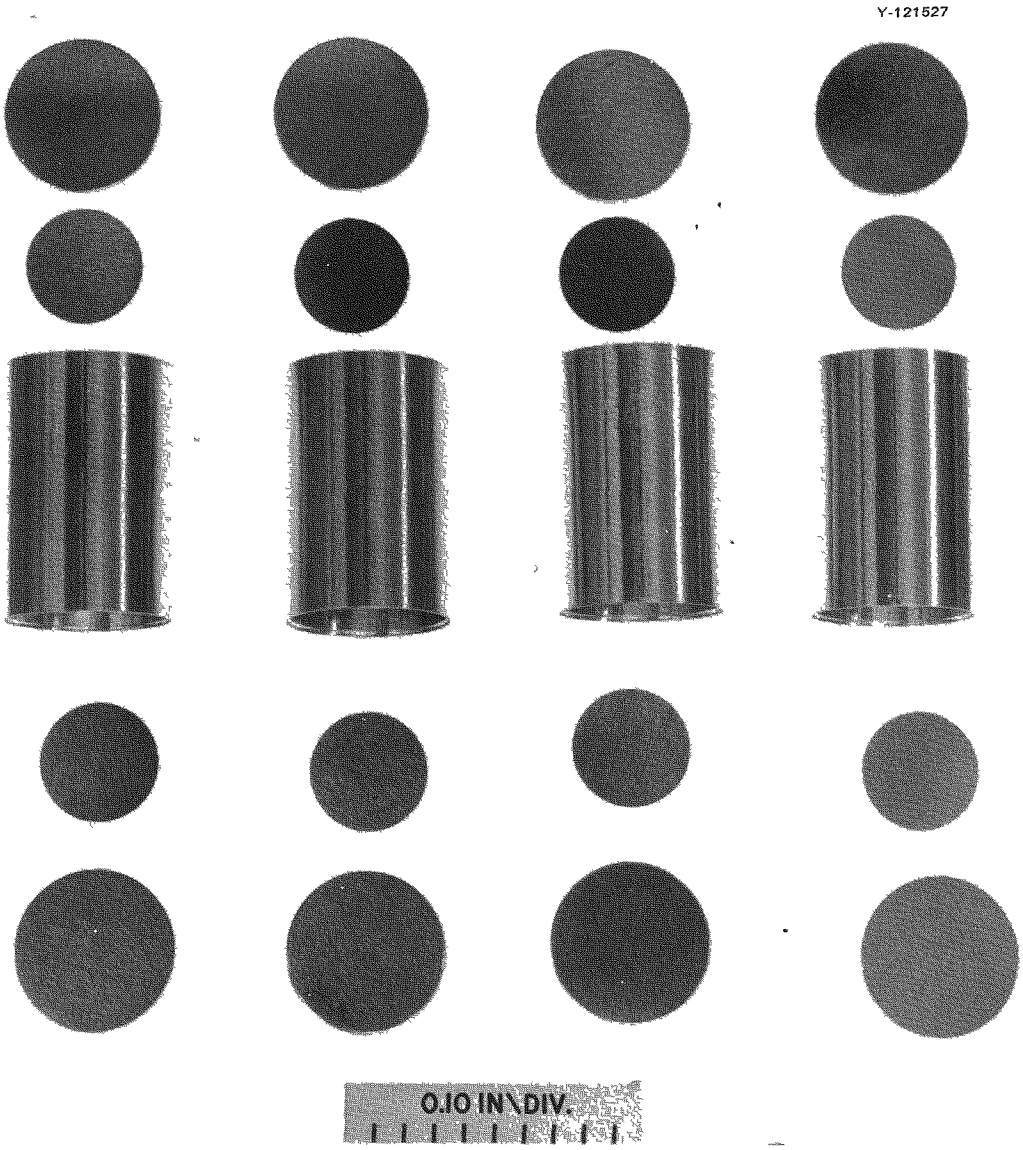

Fig. 4. Four sets of capsules fabricated from Ir-1.92% W sheet.

To explore these possibilities, strip specimens were prepared from a rejected blank, WE-22. The specimens were first annealed for 1 hr in the temperature range 1140 to 1350°C and then reannealed 1 hr at 1500°C. Metallographic examination indicates that the specimens, with or without intermediate anneal, showed some degree of abnormal grain growth after the final anneal of 1 hr at 1500°C. The abnormal grains appear as patches scattered in the base grain structure. Because abnormal grain growth has been observed in the blank material, indication is that the deformation or strain due to hemisphere forming or mishandling has nothing to do with this abnormal growth. Furthermore, in order to determine the effect of the intermediate anneal on the degree of abnormal grain growth, the grain size distribution in these specimens was analyzed

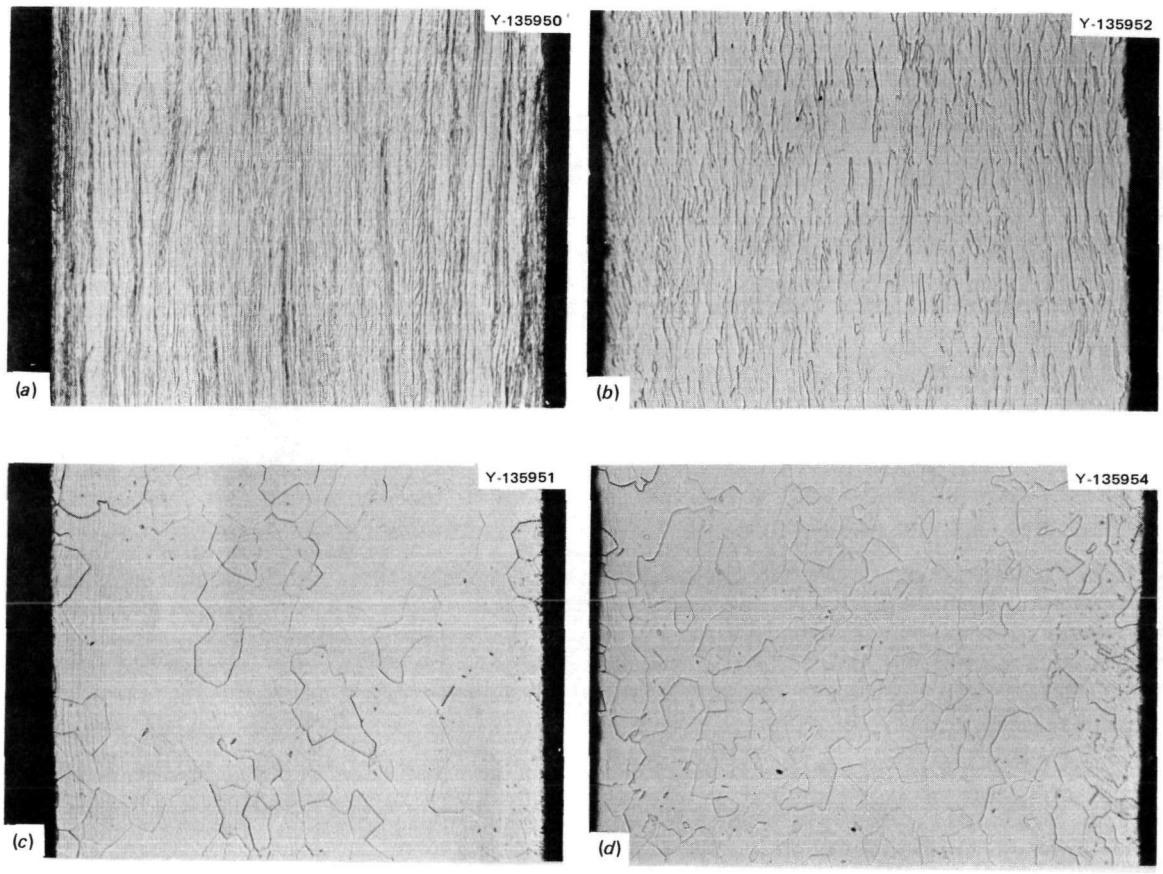

Fig. 5. Microstructures of iridium-tungsten alloys at 100X. (*a*) Ir-0.3% W (WC), as-rolled condition; (*b*) Ir-3.84% W (Ir-29), as-rolled condition; (*c*) Ir-0.3% W (WC), annealed 1 hr at 1500°C; (*d*) Ir-1.92% W (Ir-38) annealed 1 hr at 1500°C.

by quantitative metallography. The results, shown in Table 4, indicate that more than 90% of the grains are ASTM grain size 3-6. Coarse grains (ASTM 1-2) are observed in all the specimens, indicating that the intermediate anneal has only a small effect on abnormal grain growth.

The results of this annealing study indicate that the abnormal growth in WE material is due to its grain instability at high temperature. Because such grain growth is not observed in WC PICS subjected to the same heat treatment,[8] the trace impurities existing in different iridium lots are believed to play a dominant role on grain stability and grain growth at high temperatures.

A series of experiments were conducted to find a suitable method for surface cleaning and structural control in Ir-0.3% W hemispheres[5] produced by ORNL/Mound and EI processes. Contamination of surfaces with

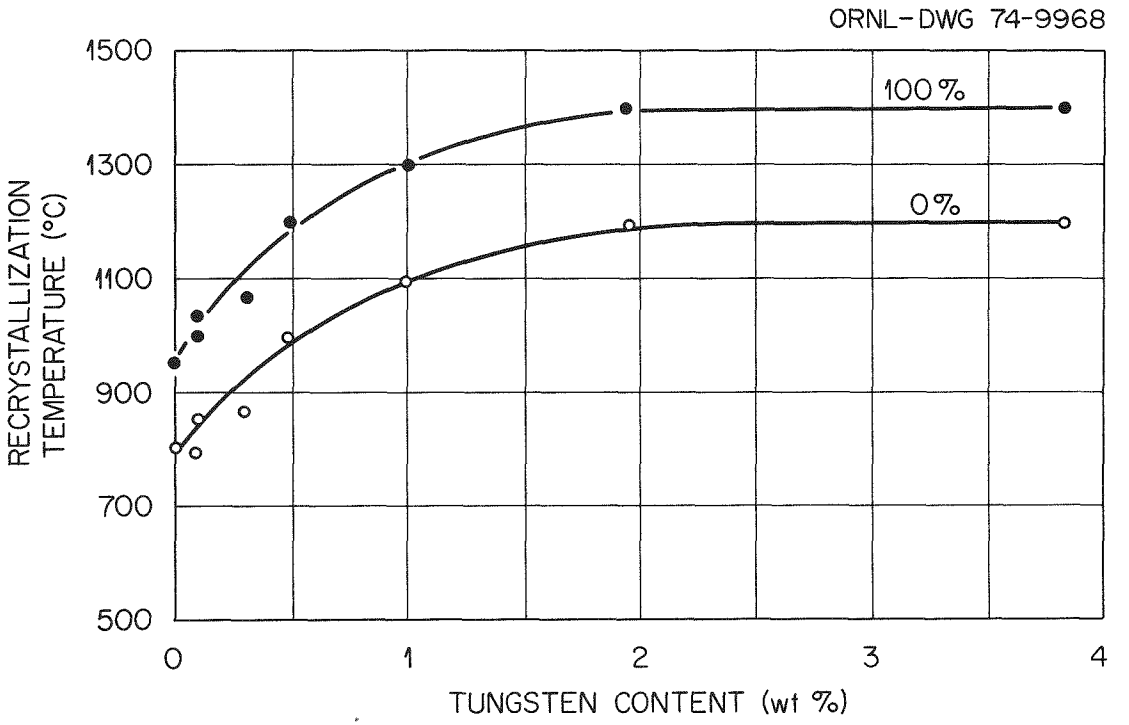

Fig. 6. Plot of recrystallization temperatures as a function of tungsten content in iridium-tungsten alloys.

Table 3. Effect of 1-hr heat treatment on grain-growth behavior of iridium-tungsten alloys

Annealing Temperature (C°)	ASTM grain size number					
	0%	0.09% W	0.3% W	0.96% W	1.92% W	3.84% W
	EBP-21	EBP-21	WC-4	Ir-19	Ir-38	Ir-29
1200	3-4	5-6	6-7	*a*	*a*	*a*
1400	2	3	5-6	6	6	6-7
1500	1-2	1-2	4-5	5	5-6	5-6
1600	1	1-2	3-4	4	4	4-5

[a]Not completely recrystallized.

Table 4. Effect of intermediate anneal[a] on the abnormal grain growth in WE-22 specimens at 1500°C[b]

Intermediate anneal temperature[a] (°C)	Distribution of ASTM grain size (%)					
	No. 6[c]	No. 5	No. 4	No. 3	No. 2	No. 1
d	22	34	18	18	7	1
1175	23	32	24	14	4	3
1250	16	31	27	20	5	1
1300	19	33	20	23	4	1

[a]For 1 hr in vacuum.

[b]For 1-hr anneal at 1500°C.

[c]Grain size equal to or smaller than ASTM grain size 6.

[d]No intermediate anneal.

impurities or coating with oxides during PICS fabrication may affect compatibility with PuO_2 fuel or cause plugging of the vent for helium release during long-term operation at 1330°C. The hemispheres produced by the Engelhard Industries process (EI-46, -52) showed a black coating on the inner surface, whereas the hemisphere produced by the ORNL/Mound process (WC-3) was bright on both surfaces. Sections of the hemispheres were heat treated in a vacuum at 900, 1100, 1300, and 1500°C for 1 hr. A section of the EI-52 hemisphere was soaked in hot HF for 4 hr followed by ultrasonic cleaning prior to vacuum anneal at 1500°C. This treatment is used to clean the sectioned hemisphere at Mound Laboratory.

Table 5 summarizes the effect of the vacuum anneals on the hardness, yield strength, and microstructure of the hemisphere sections produced by the two different processes. The products are notably different in the following aspects.

1. The hardness and yield strength of WC-3 are greater than for EI-46 in the as-fabricated condition and after a 900°C anneal.
2. The hardness and yield strength of the EI product are greater than for the ORNL/Mound product for anneals above 1100°C.
3. A duplex structure characterized by a band at the surface (0.008 to 0.0013 cm thick) is observed in the EI product (Fig. 7*a*), whereas the ORNL/Mound product shows a uniform grain structure (Fig. 7*b*).
4. The 100% recrystallization temperature of the ORNL/Mound product is between 900°C and 1100°C. A 100% recrystallization temperature for the EI product is not well defined due to the duplex structure but is estimated to be between 1100 and 1300°C.

Table 5. Effect of 1-hr vacuum anneal on hardness, yield strength, and microstructure of Ir-0.3% W hemispheres produced by ORNL/Mound (WC-3) and EI (EI-46) processes

Annealing temperature (C°)	Hardness R_A[a]	Yield strength[b] (ksi)[c]	Microstructure
			EI-46[d]
As fabricated	68.5	110.0	Fibrous and elongated grain structure near the edge, recrystallized grains in the middle; many particles and stringers
900	68	105.0	Same as above
1100	64.2	70.0	Same as above
1300	55.1	15.0	Small-grained structure near the edge and coarse-grained structure in the middle; many particles and stringers
1500	51.5	8.0	Same as above
			WC-3[e]
As fabricated	73.9	175.0	100% fibrous structure
900	70.6	130.0	A few recrystallized grains distributed uniformly through wrought matrix
1100	53.5	13.0	100% recrystallized structure
1300	52.5	8.0	100% recrystallized structure

[a] Rockwell A scale

[b] Estimate based on the R_A — yield-strength relation obtained from a series of tests on WC-4.

[c] 1 ksi = 6.89 MPa.

[d] Hemisphere of Engelhard material (lot 46) received from Mound Laboratory.

[e] Hemisphere of ORNL material received from Mound Laboratory.

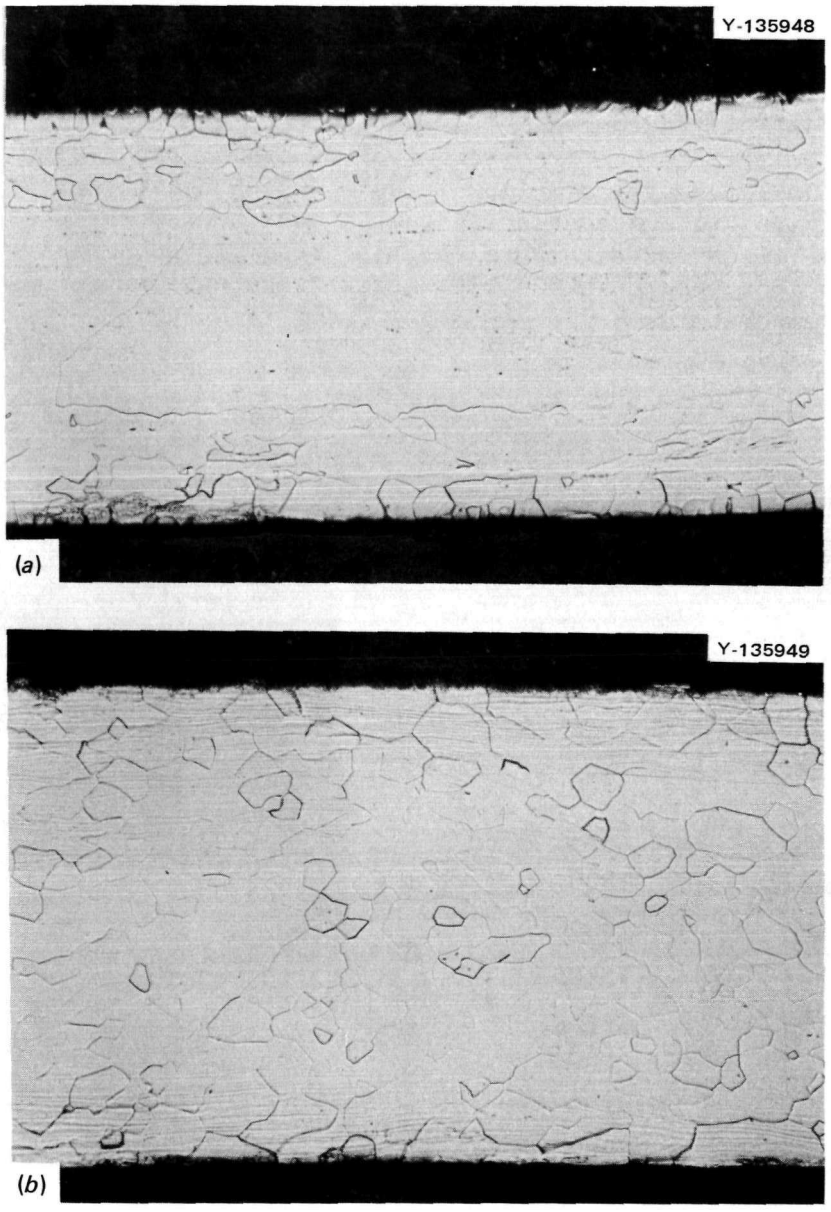

Fig. 7. Microstructure of Ir-0.3% W hemispheres produced at ORNL/Mound (WC-3) and Engelhard Industries (EI-46). Heat treatment: 1 hr at 1300°C; 100×. (*a*) EI-46: duplex grain structure; (*b*) WC-3: uniform grain structure.

Table 6 compares the interstitial content of the iridium specimens processed by the methods mentioned above. For all comparable conditions, the ORNL/Mound product contains significantly less oxygen than the EI product. A consistent decrease in the oxygen content with increased annealing temperature was observed in the EI product, whereas no further improvement occurred in the ORNL/Mound product in anneals above 900°C.

The inner surfaces of the iridium hemisphere were analyzed by SSMS after the various treatments. The results indicate that neither the annealing temperature nor prior chemical treatment had a significant effect on the level of trace impurities. Based on the results of this series of tests, recommendation is that annealing temperatures no higher than that required for structural control be employed, inasmuch as no significant improvement in the cleanness of the surface results from excessive temperatures.

Table 6. Effect of 1-hr vacuum annealing on interstitial content of Ir-0.3% W hemispheres

Hemisphere number	Annealing temperature (C°)	Interstitial content (ppm)		
		O	N	H
EI-46[a]	As fabricated[b]	32	1	<1
	900	29	1	<1
	1100	16	1	<1
	1300	15	1	<1
	1500	10	<1	<1
EI-52[c]	1500[d]	9	<1	<1
WC-3[e]	As fabricated[f]	9	<1	<1
	900	4	<1	<1
	1100	5	<1	<1
	1300	4	<1	<1

[a] A half of Engelhard hemisphere (lot 46) received from Mound Laboratory.

[b] A black coating was on the inner surface.

[c] An Engelhard hemisphere (lot 52) received from Mound Laboratory.

[d] Four-hour soak in 150°F HF plus ultrasonic clean plus 1-hr vacuum anneal at 1500°C (performed by Mound Laboratory).

[e] A half of ORNL Ir-0.3% W hemisphere received from Mound Laboratory.

[f] Both inner and outer surfaces were bright and clean.

TENSILE PROPERTIES

Tensile specimens with a gage section 0.318 cm wide by 1.3 cm long were blanked from 0.05- to 0.08-cm-thick sheets to determine tensile properties. The blanked specimens were polished on 400-A silicon carbide paper, pickled in an aqua regia plus hydrofluoric acid solution, then heat treated in a vacuum. Tensile specimens tested above room temperature were heated by radiation from an inductively heated tantalum susceptor under a vacuum of less than 1×10^{-3} Pa. A platinum vs Pt-10% Rh thermocouple centrally located on the specimen monitored the temperature. After a 10- to 15-min holding time at the test temperature, the specimens were pulled on an Instron machine at a strain rate of 0.13 to 0.51 cm/min.

Tensile Properties of Iridium Sheets

Tensile properties of iridium sheets produced by ORNL and Engelhard Industries were determined as a function of test temperature and heat treatment. Table 7 presents the tensile properties of EB iridium annealed at different conditions. The specimens in the as-rolled condition had high strength and low ductility. No significant difference in properties was noted in specimens taken longitudinally or transversely to the final rolling direction of the sheet. With increasing annealing temperature, the strength decreased, and the ductility increased. The precipitous change in the tensile properties between the specimens that were heat treated at 1100 and 1300°C is attributed to recrystallization.

Table 7. Effect of heat treatment on the room-temperature tensile properties[a] of iridium sheet EB

Heat treatment[b]	Strength (psi)[c]		Elongation (%)
	0.2% offset	Tensile	
As rolled	148,700	164,000	2.0
As rolled (transverse)	156,000	164,500	2.2
1 hr at 1100°C	117,000	190,700	10.8
1 hr at 1300°C	14,600	70,900	12.6
1 hr at 1500°C	9,500	57,000	10.9[d]

[a] Tested at a crosshead speed of 0.05 in./min.

[b] Annealed in a vacuum; all specimens longitudinal except as noted.

[c] 1 psi = 6.89×10^3 Pa.

[d] Average of two specimens.

Most tensile data were obtained from the specimens recrystallized 1 hr at 1500°C. These results are presented in Fig. 8 as a function of test temperature up to 1370°C. The tensile properties of iridium are sensitive to trace impurities existing in various sheets. Sheets EBP-21 and EB, produced by electron-beam melting at ORNL, had a low yield strength (σ_y) of 55.1 to 68.9 MPa [8 to 10 (ksi)] at room temperature, whereas the EI sheets S-65, -69 (containing higher levels of impurities) had σ_y of 117.1 to 172.3 MPa (17 to 25 ksi), which is more than twice the value for the ORNL sheets. Also, in contrast to the EI sheets, the σ_y of the ORNL sheets is independent of test temperature up to 1100°C.

The stress-strain curves of iridium exhibit unusually high work hardening rates at all test temperatures. These rates result in a tensile stress that is higher than its σ_y by 300 to 500%. The tensile strength increases with temperature up to about 600°C; beyond that temperature it decreases steeply. The ductility of iridium sheets increases steadily with test temperature up to 1100°C and then remains relatively constant.

Broken tensile specimens were examined by optical microscopy and/or scanning electron microscopy to study their fracture behavior. The fracture mode of iridium is very sensitive to test temperature and trace impurities in various sheets. The ORNL sheets fractured mainly by an intergranular mode at temperatures up to 650°C and started to exhibit a mixed mode of grain boundary separation (GBS) and transgranular fracture (TF) at 760°C. The EI sheets exhibited a mixed fracture mode as low as 500°C and essentially a TF with a high degree of secondary cracks at 650°C. These observations suggest that EI material is more resistant to brittle GBS fracture. Figure 9 compares the fracture modes of EI and ORNL materials at 760°C. The dimple-type fracture generally associated with ductile rupture is not observed on the TF surfaces; instead, the fracture surface exhibits contoured steps typical of a cleavage fracture. It should be noted that iridium is only one of the fcc metals that exhibits a cleavage-type fracture at these temperatures. All sheets, whether EI or ORNL, exhibited ductile rupture at 1093 to 1370°C. In fact, sheet specimens necked to knife edge and fractured with close to 100% reduction in area.

To study the effects of reentry heating on the tensile properties, a set of S-69 specimens were heated in a vacuum for 5 min at 2000°C after recrystallization for 1 hr at 1500°C. The results obtained at various temperatures are presented in Table 8. Comparison of the tensile data in Table 8 and Fig. 8 indicates that the heat pulse lowers the σ_y considerably but does not affect the tensile strength and ductility. The lowering in yield strength is apparently due to the coarsening of grain structure at 2000°C.

Tensile Properties of Iridium-0.3% Tungsten Alloy Sheets

The Ir-0.3% W alloy is the current PICS material for the MHW heat source; its tensile properties have been characterized extensively with emphasis on lot-to-lot and heat-to-heat variations.

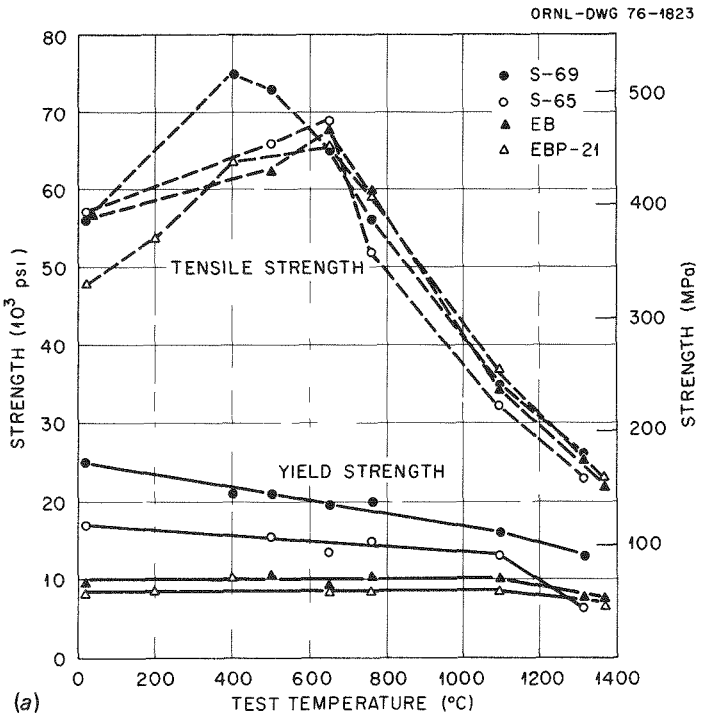

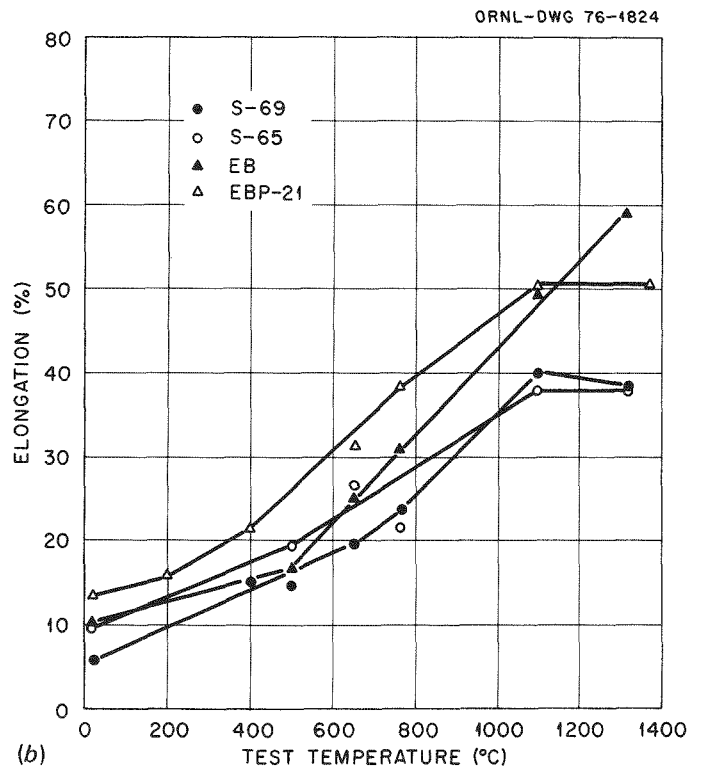

Fig. 8. Plot of tensile properties as a function of test temperature for various iridium sheets. (*a*) Yield and tensile strength; (*b*) Elongation.

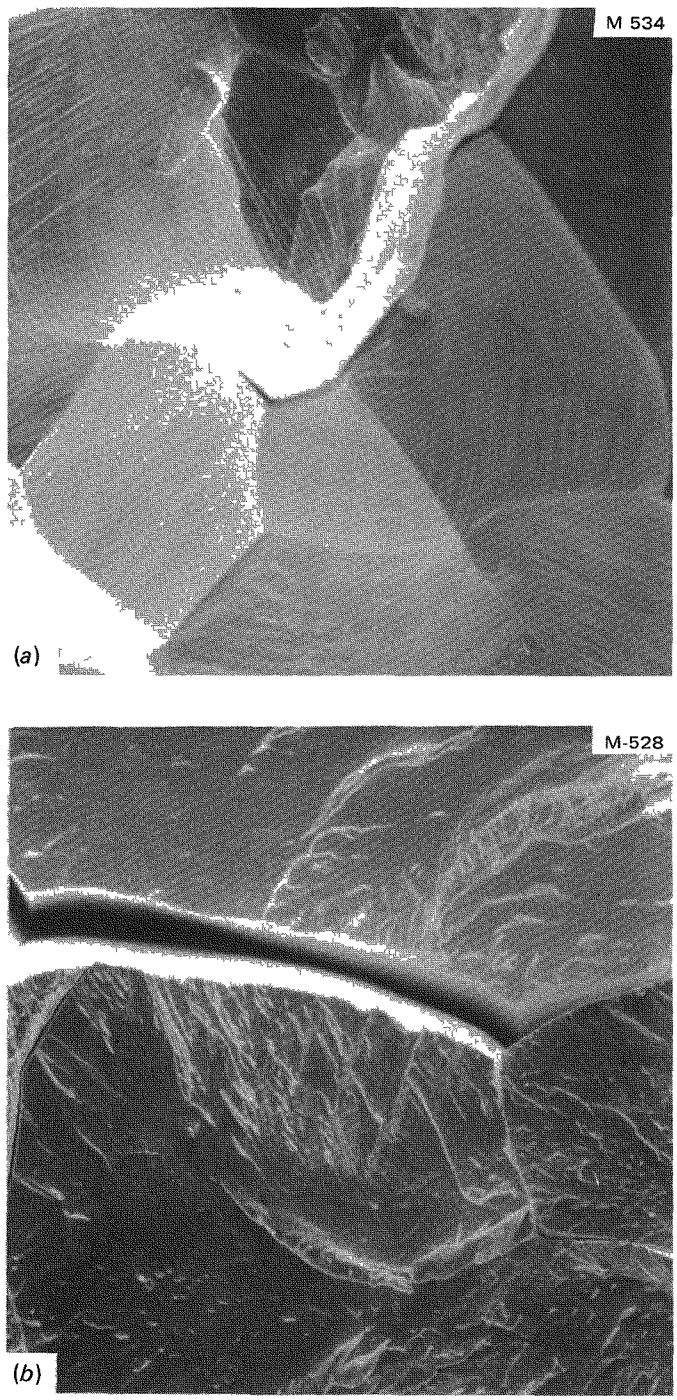

Fig. 9. Scanning electron microscope fractographs of OEP iridium and EI iridium specimens broken in tension at 760°C; 300×.

Table 8. Tensile properties[a] of S-69 sheet specimens annealed 5 min at 2000°C after recrystallization for 1 hr at 1500°C

Testing temperature (°C)	Strength (psi)[b]		Elongation (%)
	Yield	Tensile	
Room	12,500	46,100	8.5
500	17,800	61,200	17.8
760	11,500	57,000	24.3
1093	8,500	32,000	36.2
1315	10,500	23,000	33.7

[a]Tested in vacuum at a crosshead speed of 0.05 in./min.

[b]1 psi = 6.89 x 10^3 Pa.

A first series of Ir-0.3% W sheet specimens were annealed for 15 min between 850 and 1000°C and then tested at room temperature and at 800°C to determine the optimum heat treatment condition for forming Ir-0.3% W disks at Mound Laboratories. Table 9 shows the tensile results for lots WB-1 and WC-3 to -11. The WC-4 sheet annealed at 850°C had low ductility but high strength at room temperature. For the specimens tested at 800°C, the strength decreases and ductility increases with annealing temperature. The variation in properties from heat to heat is insignificant, as indicated in Table 9. All the annealed specimens exhibited some degree of necking at 800°C.

Most tensile data were obtained after a standard recrystallization treatment for 1 hr at 1500°C. Table 10 summarizes the results from ORNL and EI (S-74, EI-114) materials. The stress-strain curves of WC-4 specimens were calculated and are shown in Fig. 10. The Ir-0.3% W alloy exhibits a low yielding but a high work-hardening rate at these temperatures. The hardening rate decreases with test temperature; however, the tensile-to-yield-strength ratio remains as high as 4.7 at 1370°C. Discontinuous yield and serrated plastic flow are not observed on these curves, indicating low impurity in these electron-beam-melted OEP heats. The specimen fractured without necking at room temperature, started to show necking at 760°C, and necked significantly at 1093 and 1370°C.

The tensile data of Ir-0.3% W sheets prepared from the OEP powders are presented in Fig. 11 as a function of test temperature. The ductility of the sheets increases with test temperature. All the sheets had about 13% elongation at room temperature and more than 50% elongation at temperatures of 1093°C and above. The yield strength of the Ir-0.3% W is low and is slightly dependent on the test temperatures; however, the tensile strength decreases sharply above 760°C. All of the sheets exhibited tensile strengths between 165.4 and 179.1 MPa

Table 9. Effect of 15-min vacuum annealing on tensile properties[a] of Ir-0.3% W sheet specimens tested at room temperature and 800°C

Annealing temperature (C°)	Heat number	Strength (ksi)[b]		Elongation (%)	Reduction in area (%)
		Yield	Tensile		
		Room temperature			
850°C	WC-4	19.20	197.0	2.5	[c]
		800°C			
As rolled	WC-4	139.0	145.0	3.4	[c]
850	WC-3	123.0	137.0	5.4	[d]
	WC-4	133.0	141.0	4.3	16
	WC-11	126.0	136.0	4.9	[d]
900	WB-1	121.0	141.0	4.8	[d]
	WC-4	126.0	134.0	5.0	14
950	WC-4	110.2	120.7	6.1	19
1000	WC-4	73.0	91.3	10.0	24

[a] Tested in a vacuum at a crosshead speed of 0.05 in./min.

[b] 1 ksi = 6.89 MPa.

[c] Fractured without necking.

[d] Not measured.

(24 and 26 ksi) at 1370°C. From these results, we conclude that the tensile properties of Ir-0.3% W sheets used for production of the space nuclear flight system hardware do not vary significantly from lot to lot after a standard heat treatment of 1 hr at 1500°C.

Like those of unalloyed irridium, the yield strength and fracture behavior of Ir-0.3% W alloy are quite sensitive to trace impurity and test temperature, as indicated in Table 10. The EI sheets (S-74 and EI-114) had much higher yield strengths than the ORNL sheets at all test temperatures. Figure 12 compares the scanning electron microscope fractographs of WG and S-74 specimens fractured at 650, 760, and 1093°C. As indicated, the EI material is more resistant to intergranular fracture at lower temperatures.

Table 10. Properties[a] of Ir-10.3% W sheet specimens vacuum-annealed for 1 hr at 1500°C

Heat No.	Strength (ksi)[b] Yield	Strength (ksi)[b] Tensile	Elongation (%)	Fracture mode[c]
		Room temperature		
WC-4	13.4	55.7	12.1	Mainly GBS
WCR-93	12.3	58.1	12.9	Mainly GBS
WD-1	13.0	61.0	14.2	Mainly GBS
WE-3	13.1	60.4	12.4	Mainly GBS
WER-94	14.4	54.3	12.0	Mainly GBS
WG-202	11.8	62.6	14.0	Mainly GBS
S-74	16.0	63.2	9.7	Mainly GBS
EI-114-C	13.3	63.2	13.5	Mainly GBS
		650°C		
WC-4	12.0	58.5	23.0	Mainly GBS
WCR-93	9.5	60.1	23.3	Mainly GBS
WD-1	10.7	70.4	32.2	Mainly GBS
WE				
WER-94	9.6	70.7	33.0	Mainly GBS
WG-202	7.4	70.8	30.1	Mainly GBS
S-74	15.2	----	----	GBS and TF
EI-114-C	13.6	74.2	37.6	GBS and TF
		760°C		
WC-4	7.5	58.1	32.5	TF (Ma) and GBS (Mi)
WCR-93	8.9	64.6	39.8	GBS and TF
WD-1	9.3	58.7	42.5	Mainly TF
WE-3	11.0	65.6	34.0	GBS (Ma) and TF (Mi)
WER-94	8.6	59.1	42.1	GBS (Mi) and TF (Mi)
WG-202	6.8	64.0	39.3	GBS (Ma) and TF (Ma)
S-74	16.0	60.5	25.0	Completely TF
EI-114-C	15.4	64.0	38.6	Mainly TF
		1093°C		
WC-4	7.3	35.0	53.5	DR
WCR-93	6.5	40.1	57.6	DR
WD-1	10.6	36.8	55.3	DR
WE-3	7.9	34.9	51.5	DR
WER-94	----	35.0	56.7	DR
WG-202	6.7	36.2	55.6	DR
S-74	17.0	51.2	37.5	DR
EI-114-C	10.5	39.0	56.0	DR
		1316°C		
WC-4	4.5	24.7	44.5	DR
WC-3	5.5	26.5	60.7	DR
WC-1	5.1	25.7	57.6	DR
WC-11	4.9	26.4	54.2	DR
S-74	10.5	27.6	47.0	DR
		1370°C		
WC-4	5.2	24.4	50.4	DR
WCR-93	5.0	26.3	54.2	DR
WD-1	7.8	23.8	56.0	DR
WE-3	7.9	25.5	55.7	DR
WER-94	6.1	24.3	53.4	DR
WG-202	5.6	25.8	55.2	DR
S-74				
EI-114-C	10.3	26.4	54.0	DR

[a] Tested in vacuum at a crosshead speed of 0.05 to 0.2 in./min.

[b] 1 ksi = 6.89 MPa.

[c] GBS, grain boundary separation; TF, transgranular fracture; Ma, major fraction; Mi, minor fraction; and DR, ductile rupture.

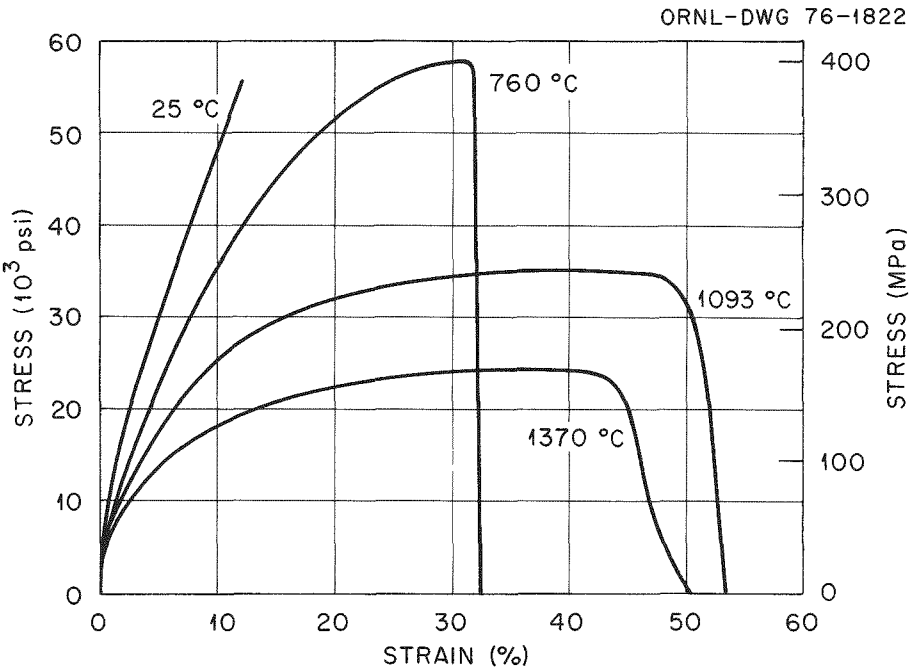

Fig. 10. Stress-strain curves of Ir-0.3% W alloy sheet (WC-4) tested at 25, 760, 1093, and 1370°C.

Tensile Properties of Iridium-Tungsten Alloys

The tensile properties of iridium-tungsten alloys heat treated for 1 hr at 1500°C are presented in Table 11 and are plotted as a function of tungsten content at five test temperatures in Fig. 13. The iridium-tungsten alloys prepared from EI material had higher yield strength and slightly lower ductility than the alloys prepared from OEP iridium powder, so their tensile data were not included in the plots. The yield strength increases almost linearly with tungsten content at these temperatures, indicating the hardening of iridium with added tungsten. The tensile strength also increases with tungsten content except for the points above 2% W at 650 and 760°C. The elongation of the alloys decreases with the tungsten content at room temperature and at 650, 760, and 1093°C, but it remains at a constant level of 50% at 1370°C until the tungsten content is over 2%. The iridium-tungsten alloys are compared in Fig. 14 in terms of toughness, defined as the product of fracture strain and half the sum of tensile strength and yield strength at 1370°C, the projected MHW fuel sphere assembly impact temperature. The toughness of Ir-1.92% W is 13,900 in.-lb/in.^{3}, which is the highest among the alloys. The high toughness of Ir-1.92% W is derived from both good strength and ductility at 1370°C. Thus, this alloy possesses the most promising mechanical properties among the alloys in this investigation.

The fracture surface of iridium-tungsten specimens was examined by optical microscopy and scanning electron microscopy; the results are also presented in Table 11. The alloys prepared from the OEP powder

Table 11. Tensile properties[a] of iridium-tungsten sheet specimens vacuum-annealed for 1 hr at 1500°C

Alloy (wt %)	Strength (ksi)[b] Yield	Strength (ksi)[b] Tensile	Elongation (%)	Fracture behavior[c]
		Room temperature		
Ir (EBP-21)	8.2	48.0	13.6	Mainly GBS
Ir-0.1 W (Ir-32)	8.9	45.3	12.0	Mainly GBS
Ir-0.3 W (WC-4)	13.4	55.7	12.1	Mainly GBS
Ir-0.5 W (Ir-33)	13.8	54.6	13.2	Mainly GBS
Ir-0.96 W (Ir-19)	29.1	56.0	6.8	Mainly GBS
Ir-1.92 W (Ir-38)	32.8	64.0	8.4	Mainly GBS
(Ir-15)	36.7	70.3	8.3	Mainly GBS
Ir-3.8 W (Ir-29)	51.7	64.0	4.0	Mainly GBS
		650°C		
Ir	8.6	65.2	31.1	Mainly GBS
Ir-0.1 W	9.9	58.2	25.8	Mainly GBS
Ir-0.3 W	12.0	65.5	23.0	Mainly GBS
Ir-0.5 W	9.7	65.5	26.1	Mainly GBS
Ir-0.96 W				TF and GBS
Ir-1.92 W (Ir-38)	20.2	76.7	20.2	Mainly GBS
Ir-1.92 W (Ir-15)	23.5	72.2	16.0	Mainly GBS
Ir-3.84 W	33.8	62.5	8.5	Mainly GBS
		760°C		
Ir (EBP-21)	8.2	56.9	38.4	GBS and TF
Ir-0.1 W	7.3	53.5	36.0	GBS and TF
Ir-0.3 W	7.5	58.1	32.5	TF (Ma) and GBS (Mi)
Ir-0.5 W	9.5	58.4	34.3	TF (Ma) and GBS (Mi)
Ir-0.96 W	23.6	58.0	24.4	Mainly TF
Ir-1.92 W (Ir-38)	21.2	79.8	29.1	Mainly GBS
Ir-1.92 W (Ir-15)	22.2	84.2	30.0	GBS (Ma) and TF (Mi)
Ir-3.84 W	30.0	57.3	10.6	Mainly GBS
		1093°C		
Ir	8.5	37.0	50.6	DR
Ir-0.1 W	6.8	34.2	47.7	DR
Ir-0.3 W	7.3	35.0	53.5	DR
Ir-0.5 W	9.2	35.0	49.4	DR
Ir-0.96 W	21.0	40.0	41.8	DR
Ir-1.92 W (Ir-38)	20.4	55.2	40.2	DR
Ir-1.92 W (Ir-15)	22.2	60.5	31.2	DR
Ir-3.84 W	25.3	56.9	22.3	DR, TF
		1370°C		
Ir	7.4	23.0	50.4	DR
Ir-0.1 W	6.0	23.1	52.2	DR
Ir-0.3 W	5.2	24.4	50.4	DR
Ir-0.5 W	7.0	25.7	50.5	DR
Ir-1.92 W (Ir-38)	15.3	38.0	52.3	DR
Ir-1.92 W (Ir-15)	18.0	45.1	42.0	DR
Ir-3.84 W	21.7	46.9	25.1	DR

[a] Tested in a vacuum at a crosshead speed of 0.05 to 0.2 in./min.

[b] 1 ksi = 6.89 MPa.

[c] GBS, grain boundary separation; TF, transgranular fracture; DR, ductile rupture; Ma, major fraction; and Mi, minor fraction.

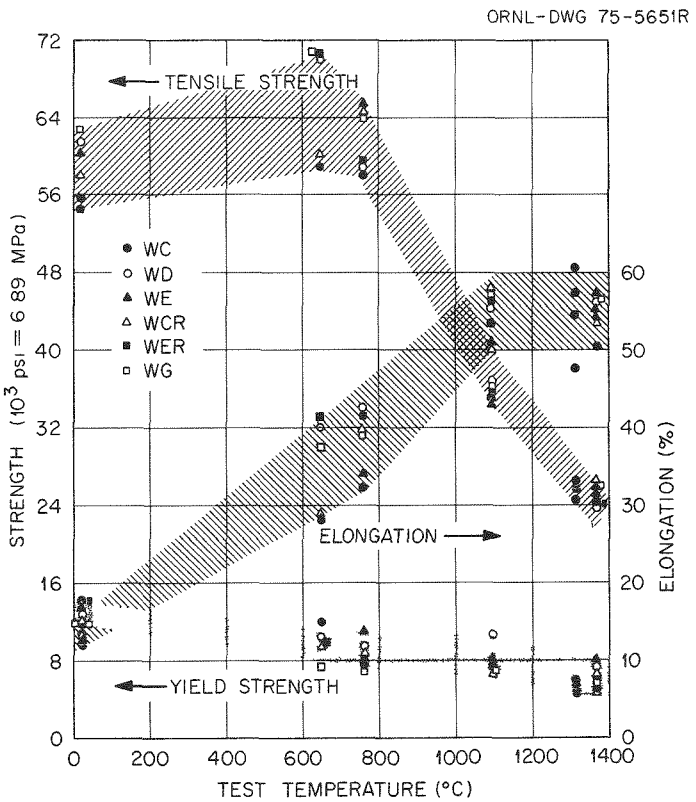

Fig. 11. Tensile properties of Ir-0.3% W sheets as a function of test temperature.

fractured mainly by GBS at room temperature and 650°C. At 760°C the alloy with less than 1% W exhibited mixed modes of GBS and TF, whereas the alloys with more than 1% W fractured mainly by GBS. Thus alloying with tungsten does not improve the fracture behavior. The iridium-tungsten alloys prepared from the EI material are more resistant to GBS at low temperatures. All the alloys exhibited ductile rupture with close to 100% reduction in area at temperatures of 1093 and 1370°C.

Tensile Properties of Notched Specimens

To study the notch sensitivity, specimens of Ir-0.3% W and Ir-1.92% W alloys were prepared with a groove 0.015 cm wide by 0.079 cm long on both sides. The notched specimens were then annealed for 18 hr at 1500°C in contact with graphite. The results of tensile tests at 1370°C are presented in Table 12. The alloy specimens had an overall elongation of 12 to 16%. The elongation actually reached a level of 1000% if the width of the notch is considered as the gage length. Examination of the

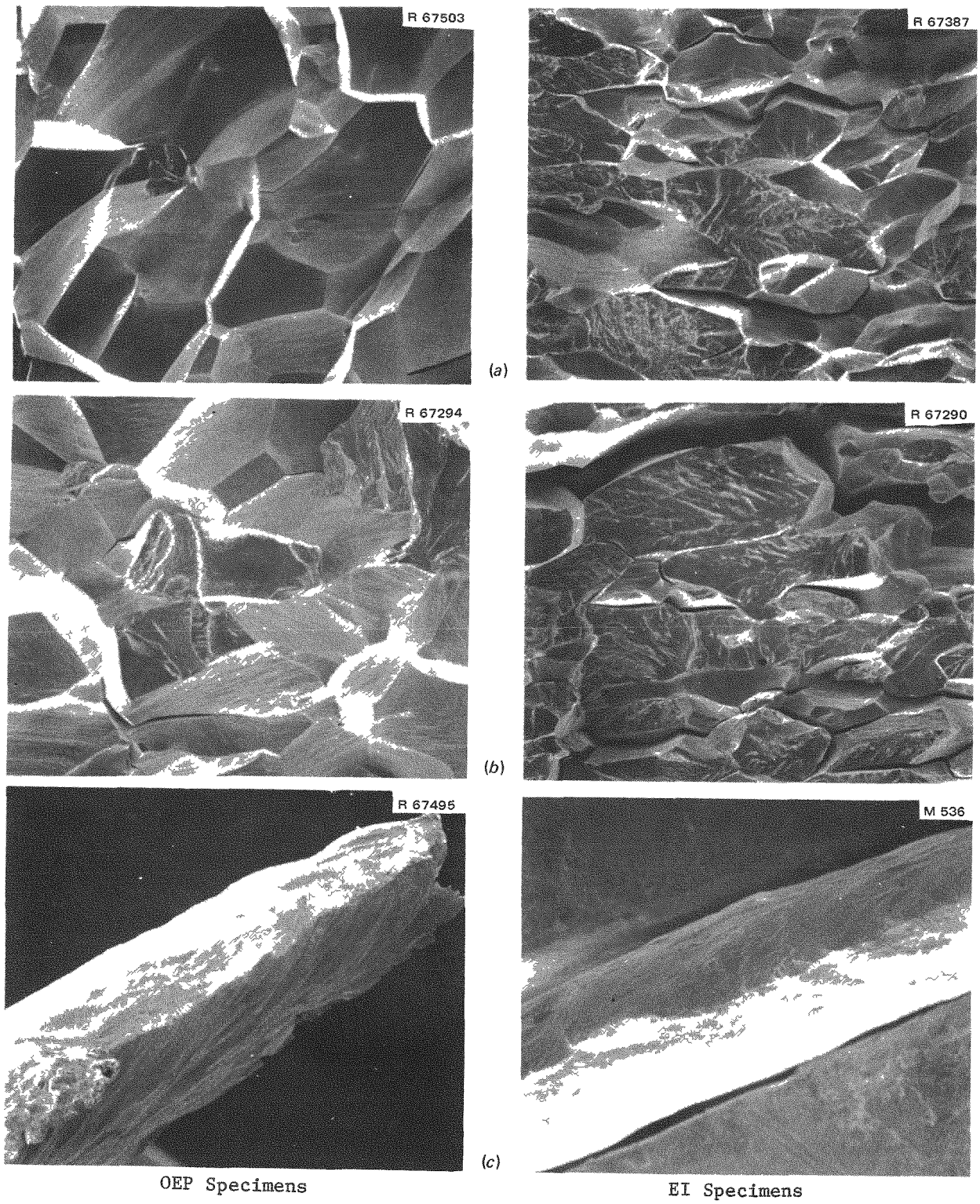

Fig. 12. Scanning electron microscope fractographs of OEP sheet and EI sheet specimens broken in tension at (*a*) 650, (*b*) 760, and (*c*) 1093°C. Fractographs shown at 300×.

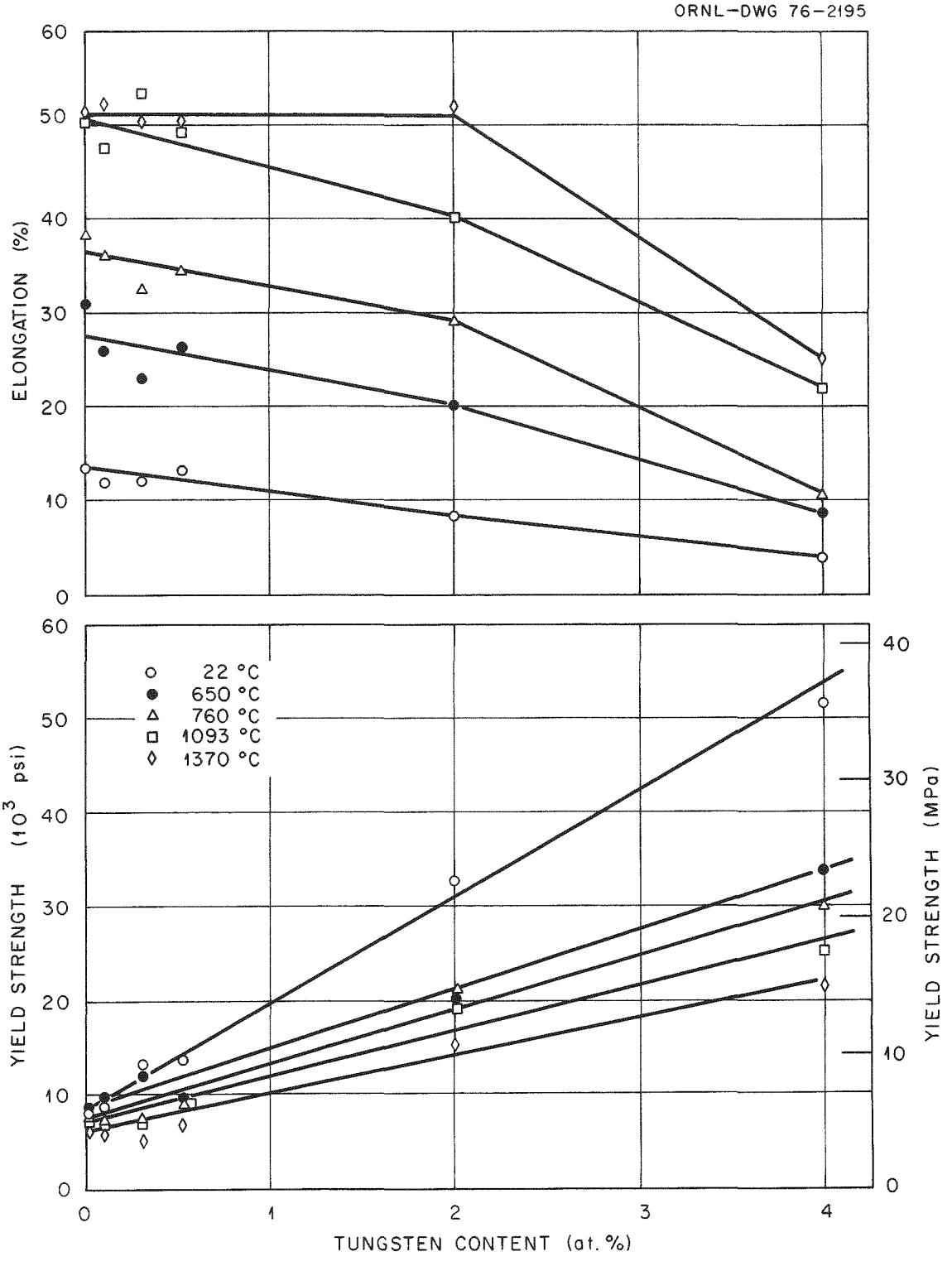

Fig. 13. Tensile properties of iridium-tungsten alloys as a function of tungsten content.

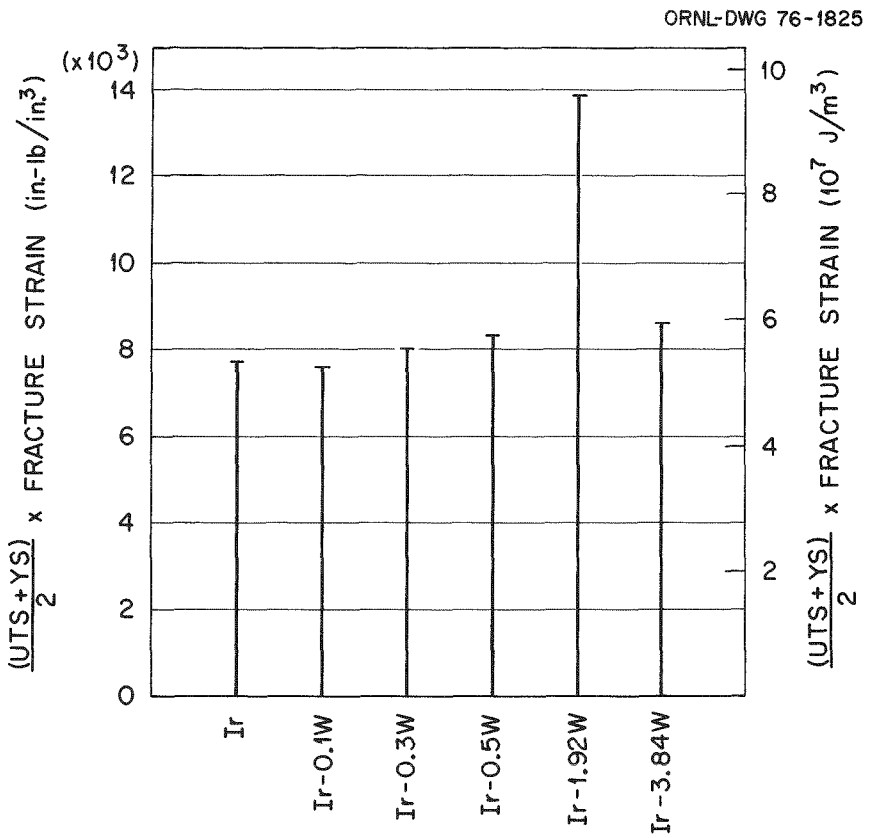

Fig. 14. Toughness of iridium-tungsten alloys.

fracture surfaces showed that the specimens necked to knife edge and fractured by ductile rupture. These results indicate that the iridium-tungsten alloys are not notch-sensitive at 1370°C. According to the Bridgman analysis,[9] a component of hydrostatic tension will be induced on the notched portion when the specimen is tested under simple tension. Thus, the excellent ductility of the notched specimen demonstrates that a change of deformation state from uniaxial tension to a more complicated stress state has no adverse effect on the ductility and fracture mode.

Effect of Hydrogen Treatment on the Tensile Properties

The iridium-tungsten alloys generally contain up to 10 ppm oxygen and 20 ppm carbon, as shown in Table 1. The early works[10,11] by field-ion microscopy and Auger analysis suggest that oxygen and carbon may segregate on grain boundaries and damage the grain-boundary structure. In an attempt to remove the interstitials, a set of WC-1 sheet specimens

Table 12. Tensile properties[a] of notched iridium-tungsten sheet specimens[b] tested at 1370°C

Alloy (wt %)	Strength (ksi)[c] Yield	Strength (ksi)[c] Tensile	Elongation (%)	Fracture mode
Ir-2 W[d]	26.5	53.5	12.0	Ductile rupture
Ir-0.3 W[e]	10.7	30.8	16.0	Ductile rupture

[a]Tested in a vacuum at a crosshead speed of 0.2 in./min.

[b]All sheet specimens contacted with ATJ graphite on one side and annealed 18 hr at 1500°C prior to testing.

[c]1 ksi = 6.89 MPa.

[d]Heat No. Ir-38.

[e]Heat No. WC-3.

(0.076 cm thick) recrystallized for 1 hr at 1500°C were heat treated for 256 hr at 1100°C in 1 atm of hydrogen. Vacuum fusion analysis indicates that the hydrogen treatment did not alter the bulk oxygen content but reduced the bulk carbon content from 9 to 5 ppm. The treated specimens were tested at temperatures to 1370°C. The results are presented in Table 13 together with those obtained from the untreated specimens. The specimens, with or without hydrogen treatment, had about the same level of strength and elongation at all temperatures. Furthermore, the treated and untreated specimens exhibited the same fracture mode at low temperatures, indicating no improvement of fracture behavior by hydrogen treatment.

OXIDATION CHARACTERISTICS IN AIR

The air oxidation behavior of iridium and of Ir-1.92% W and Ir-3.84% W alloys was determined at 770, 870, and 1000°C, which represent the postimpact temperature range for the MHW fuel sphere assembly. Rectangular sheet specimens 0.064 cm thick were polished through 1/0 paper, pickled in aqua regia, vacuum annealed for 1 hr at 1500°C, and then oxidized in air at a flow rate of 100 liters/hr. The oxidation at 1000°C was terminated after an exposure of approximately 400 hr because of the high oxidation rate. The oxidation at 770 and 870°C was extended to approximately 1800 hr. The specimens were periodically removed from the furnace and weighed on an analytical balance with a sensitivity of 10^{-6} g.

Brown oxide coatings, probably IrO_2, gradually appeared on the specimen surface at all temperatures; however, the coating was not adherent and began to flake off after a short exposure at 1000°C. All

Table 13. Effect of hydrogen treatment on the tensile properties of Ir-0.3% W sheet specimens[a]

Hydrogen treatment[b]	Strength (ksi)[c]		Elongation (%)	Fracture behavior[d]
	Yield	Tensile		
		Room temperature		
No	12.3	58.1	12.9	Mainly GBS
Yes	12.2	62.9	14.5	Mainly GBS
		650°C		
No	9.5	60.1	23.3	Mainly GBS
Yes	9.8	70.9	34.6	Mainly GBS
		760°C		
No	8.9	64.6	39.8	GBS and TF
Yes	9.1	63.0	38.6	GBS and TF
		1093°C		
No	6.5	40.1	57.6	DR
Yes	6.6	37.8	55.5	DR
		1370°C		
No	5.0	26.3	54.2	DR
Yes	5.7	25.4	42.5	DR

[a]WC specimens annealed 1 hr at 1500°C.

[b]Heat treatment for 256 hr at 1100°C in 1 atm of hydrogen.

[c]Tested at a crosshead speed of 0.1 to 0.2 in./min in a vacuum. 1 ksi = 6.89 MPa.

[d]GBS, grain-boundary separation; TF, transgranular fracture; DR, ductile rupture.

specimens exhibited weight losses due to formation of a volatile oxide, IrO_3. The mechanisms of oxidation[12,13] appear to be

$$Ir(s) + O_2 \rightleftarrows IrO_2(s) \quad (1)$$

and

$$2IrO_2(s) + O_2 \rightleftarrows 2IrO_3(g) \quad (2)$$

Figure 15 shows the plot of the weight loss as a function of time at 770, 870, and 1000°C. Generally, a transient period of decreasing reaction rate precedes a constant reaction rate at 770 and 870°C. The

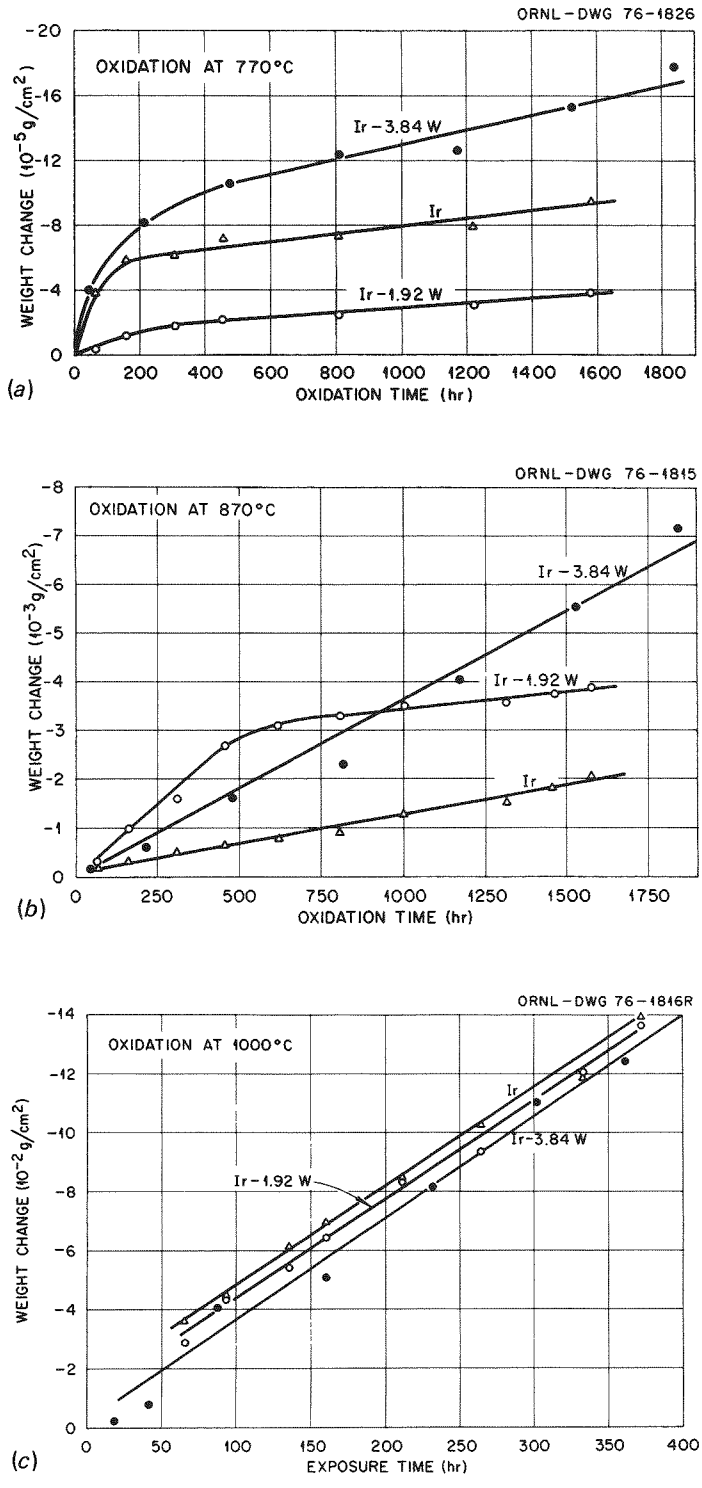

Fig. 15. Air oxidation of iridium-tungsten alloys. (*a*) 770°C, (*b*) 870°C, (*c*) 1000°C.

reaction rate constants for the linear oxidation periods are presented in Table 14 and compared with those for unalloyed iridium reported by Phillips.[14] The Ir-1.92% W alloy has the lowest linear oxidation rate — lower than for pure iridium by a factor of 2 and Ir-3.84% W by a factor of 4 at 770 and 870°C. However, the oxidation rate constants are approximately the same for the three specimens at 1000°C, indicating that alloying with up to 4% W does not alter the oxidation of iridium at this temperature. As shown in Table 14, the oxidation rate of iridium measured here at 1000°C has the same order of magnitude as reported by Phillips.[14] However, the rate is lower than that of Phillips by more than two orders at 870°C and by four orders at 770°C. This big discrepancy is believed to be due to the fact that Phillips' data were obtained from short-term oxidation (within 24 hr) and that the rate he reported was actually corresponding to the transient portion of the weight-loss-time curves as shown in Fig. 15*a* and *b*.

Table 14. Comparison of linear air oxidation rate[a] of iridium and iridium-tungsten alloys

Alloy (wt %)	Oxidation rate ($\mu g\ cm^{-2}\ hr^{-1}$)			Source
	770°C	870°C	1000°C	
Ir	0.024	1.23	310	Present work
Ir-1.92 W	0.014	0.69	310	Present work
Ir-3.84 W	0.045	3.46	340	Present work
Ir	300	400	500	Phillips[b]

[a]At an air flow rate of 100 liters/hr.

[b]W. L. Phillips, *ASM Trans. Q.* 57: 33-37 (1964).

The microstructures of the iridium-tungsten alloys after air oxidation for approximately 1700 hr at 770 and 870°C are shown in Figs. 16 and 17. Figure 18 shows the microstructure of the alloys oxidized for approximately 370 hr at 1000°C. No evidence of reaction is observed for iridium and Ir-1.92% W specimens at 770 and 870°C, whereas the Ir-3.84% W specimens exhibit grain-boundary attack at 870°C (Fig. 17*c*). The oxidation at 1000°C results in surface roughness and grain-boundary attack, as shown in Fig. 18. Some grains at the surface fell off during oxidation at 1000°C as a result of severe grain-boundary attack, as evidenced in Fig. 18*c*. This phenomenon is probably the cause of the unusual scatter in weight change data for Ir-3.84% W at 1000°C.

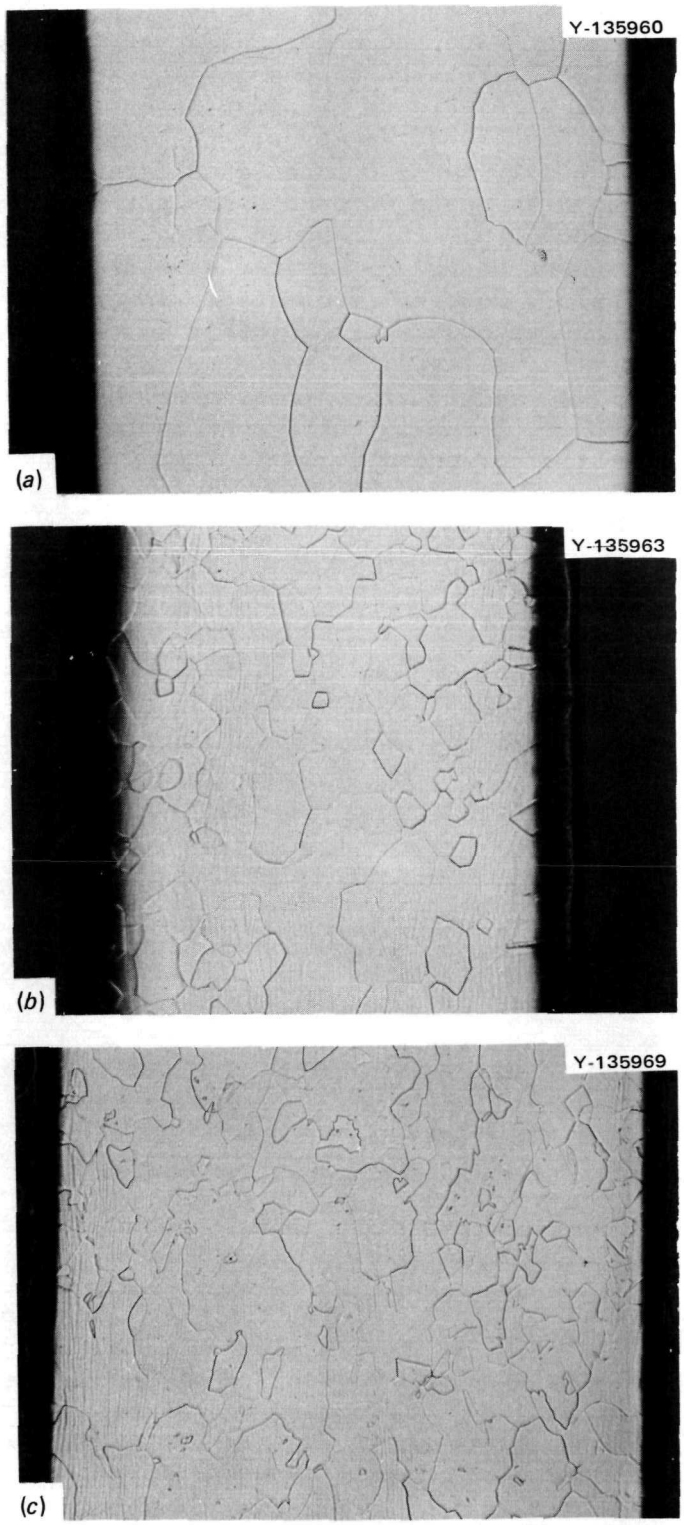

Fig. 16. Microstructures of iridium-tungsten specimens oxidized in air at 770°C for about 1700 hr; 1000×. (*a*) Iridium specimen, (*b*) Ir-1.92% W specimen, and (*c*) Ir-3.84% W specimen.

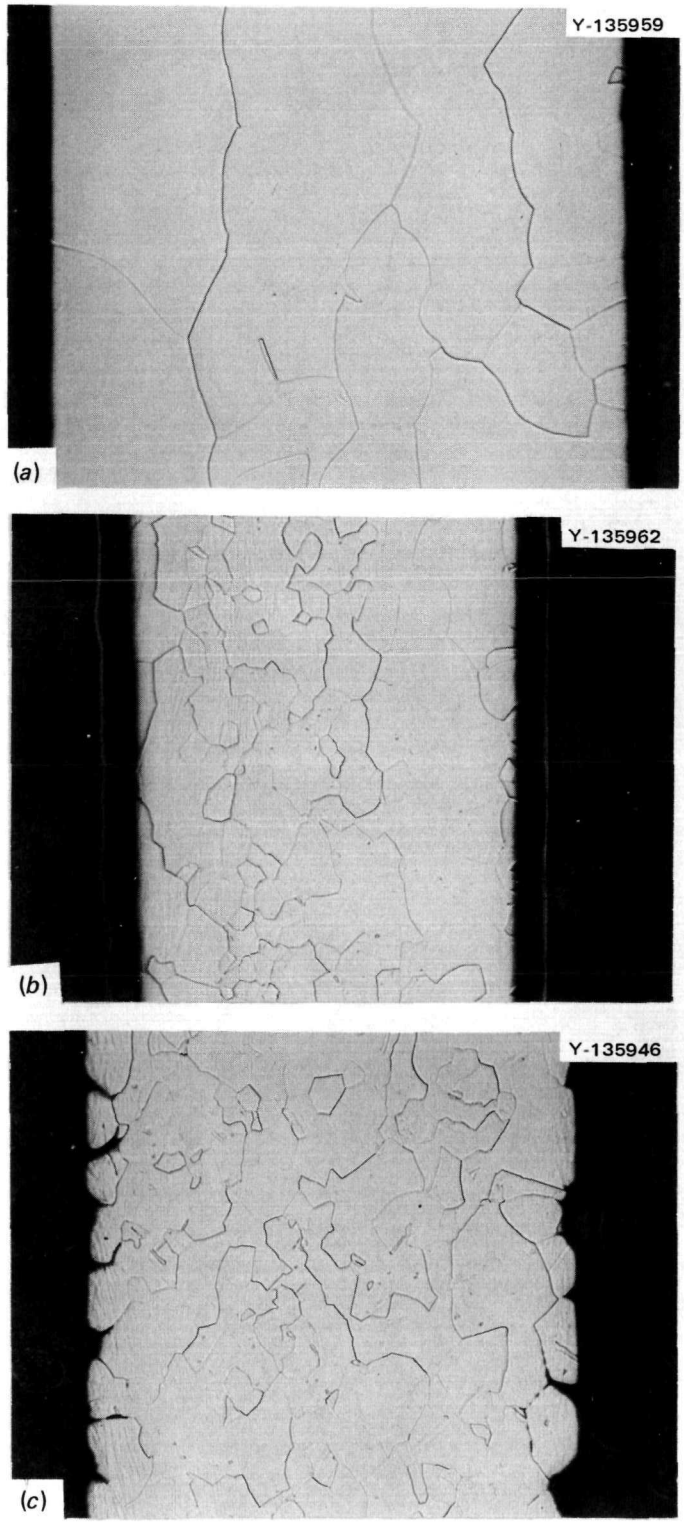

Fig. 17. Microstructures of iridium-tungsten specimens oxidized in air at 870°C for about 1700 hr; 100x. (*a*) Iridium specimen, (*b*) Ir-1.92% W specimen, and (*c*) Ir-3.84% W specimen.

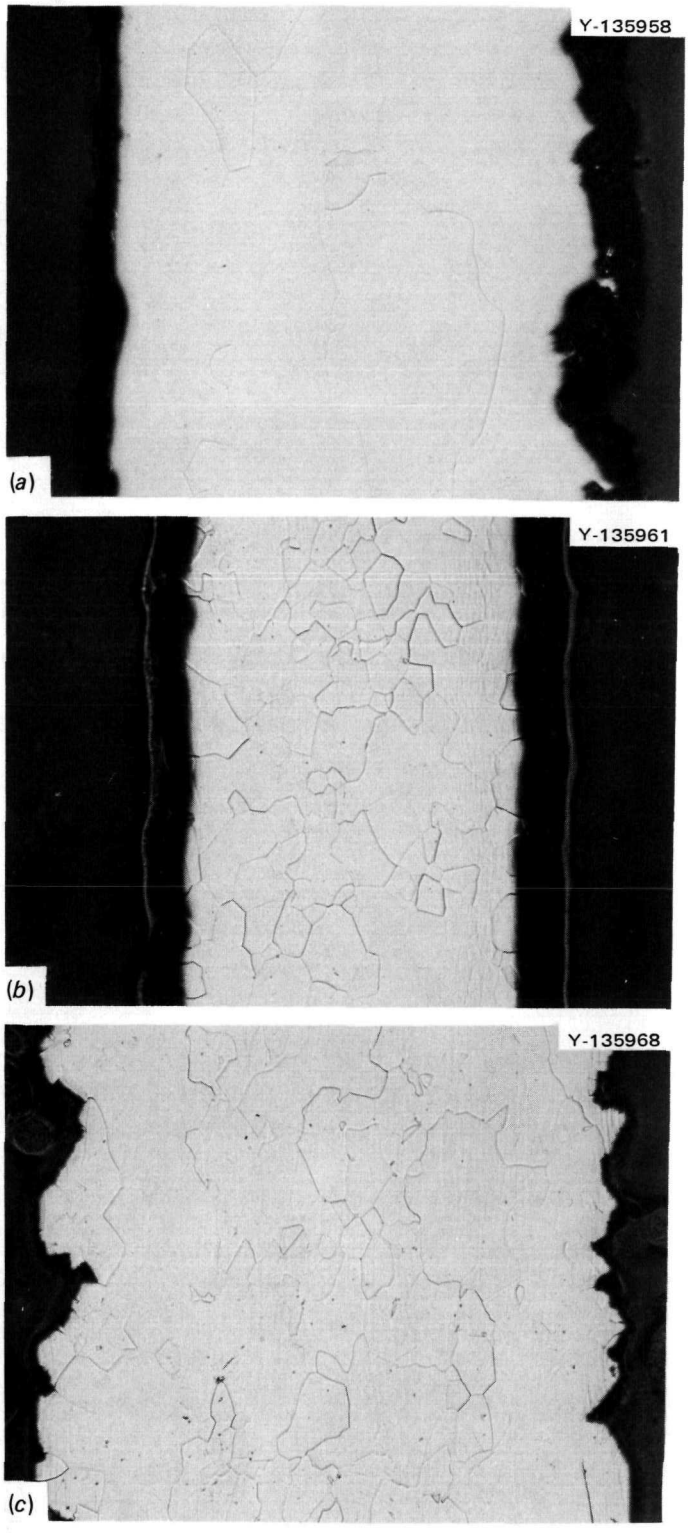

Fig. 18. Microstructures of iridium-tungsten specimens oxidized in air at 1000°C for about 370 hr; 100×. (*a*) Iridium specimen, (*b*) Ir-1.92% W specimen, and (*c*) Ir-3.84% W specimen.

The interstitial content in the oxidized specimens shown in Figs. 16 through 18 was determined by chemical analysis. To eliminate the surface effect, the chemical analysis was made on specimens whose oxide coating was removed by electropolishing. The results are presented in Table 15. The iridium and Ir-1.92% W specimens showed no increase in oxygen content after oxidation, indicating that the oxygen solubility is 5 ppm or lower at these temperatures. The Ir-3.8% W specimens picked up a small amount of oxygen (16 to 32 ppm) during oxidation. (This amount of oxygen is too small to affect the weight change of Ir-3.84% W alloy during oxidation.) The higher oxygen content in the oxidized specimens may be a result of oxygen penetration along grain boundaries (see Figs. 17*c* and 18*c*) or may be due to an increase in oxygen solubility in iridium by alloying with 4% W.

Table 15. Effect of air oxidation on the interstitial content in iridium-tungsten sheet specimens

Air oxidation condition[a]		Alloy (wt %)	Interstitial content[b] (ppm)		
Temperature (C°)	Time (hr)		O	N	H
1000	382	Ir (S-65)	5	1	1
1000	382	Ir-1.92 W (Ir-15)	5	1	2
1000	371	Ir-3.84 W (Ir-29)	38	1	1
870	1574	Ir	3	1	1
870	1574	Ir-1.92 W	3	1	1
870	1836	Ir-3.84 W	26	4	1
770	1582	Ir	4	1	1
770	1582	Ir-1.92 W	2	1	2
770	1836	Ir-3.84 W	18	1	1
As recrystallized		Ir	9	1	1
As recrystallized		Ir-1.92 W	8	1	1
As recrystallized		Ir-3.84 W	2	1	<1

[a] At an air flow rate of 100 liters/hr.

[b] Obtained by vacuum-fusion analysis.

COMPATIBILITY WITH HEAT SOURCE ENVIRONMENTS

The cladding material used in the MHW heat source is required to contact oxide fuel (PuO_2) on one side and graphite on the other side during operation and reentry from space. The environment of such a heat source operating at 1300 to 1350°C generally consists of low-pressure active gases derived from the decomposition of the oxide fuel and the outgassing of graphite and insulator materials. The reentry heating pulse could be as high as 2000°C.

Compatibility with Graphite

To determine the melting temperature between graphite and iridium-tungsten alloys, disk specimens of iridium and Ir-1.92% W alloy were stamped from the alloy sheets, polished with silicon carbide paper, and pickled in aqua regia. The specimens were then contacted with graphite coupons and heated rapidly to the desired temperature in a graphite crucible by thermal radiation from an inductively heated tungsten susceptor. The holding time was 10 min at temperatures of 2100 to 2300°C. The iridium and iridium-tungsten alloys did not bond or melt at 2250°C but did melt at 2300°C, indicating that incipient melting occurs between the alloy and graphite at 2275 ± 25°C. This demonstrates that the reentry capacity of the iridium-tungsten alloys is at least 2250°C. The incipient melting temperature determined here is close to the eutectic temperature of iridium and carbon, which has been reported[15,16] to be 2110 to 2296°C.

To study the effect of possible carbon pickup on the mechanical properties, the tensile sheet specimens of Ir-0.3% W (WCR-94) were contacted with graphite and heated together at 1500°C for 18 hr. The specimens were then tested at room temperature and at 760 and 1370°C; the results are shown in Table 16. The specimens exposed to graphite showed lower ductility at room temperature and 760°C, as compared with the specimens vacuum-annealed for 1 hr at 1500°C without exposure to graphite. The ductilities of the exposed and unexposed specimens were not different at 1370°C. The specimens showed the same fracture mode at room temperature and 1370°C but had a higher propensity for GBS at 760°C. Because Auger[17] and SSMS analysis indicate no significant change in interstitial content in bulk material or on grain boundaries, the small difference in elongation and fracture behavior of the graphite-exposed specimens presumably results from longer annealing time at 1500°C, which effects the grain size, as shown in the footnotes in Table 16.

Compatibility with Low-Pressure Active Gases

Tensile specimens of the iridium-tungsten alloys were exposed to low-pressure oxygen or oxygen and carbon environments in order to study their effects on mechanical properties. The 0.64-cm-thick sheet specimens of iridium (S-65) and Ir-0.3% W (S-74) were recrystallized for 1 hr

Table 16. Tensile properties[a] of Ir-0.3% W sheet specimens heat treated at 1500°C with or without contact with graphite

Heat number	Strength (ksi)[b]		Elongation (%)	Fracture behavior[c]
	Yield	Tensile		
		Room temperature		
WCR-93[d]	12.3	58.1	12.9	Mainly GBS
WCR-94[e]	11.6	46.5	10.7	Mainly GBS
		760°C		
WCR-93[d]	8.9	64.6	39.8	GBS and TF
WCR-94[e]	7.3	60.5	28.9	GBS (Ma) and TF (Mi)
		1370°C		
WCR-93[d]	5.0	26.3	54.2	Ductile rupture
WCR-94[e]	6.5	25.2	51.9	Ductile rupture

[a]Tested in vacuum at a crosshead speed of 0.1 to 0.2 in./min.

[b]1 ksi = 6.89 MPa.

[c]GBS, grain-boundary separation; TF, transgranular fracture; Mi, minor fraction; and Ma, major fraction.

[d]Specimens were annealed for 1 hr at 1500°C without contact with graphite. The grain size was ASTM grain size No. 4-5; the interstitial content was 4 ppm O_2 and 8 ppm C.

[e]Specimens were annealed for 18 hr at 1500°C in contact with graphite on both sides. The grain size was ASTM grain size No. 1-3; the interstitial content was 6.6 ppm O_2 and 11 ppm C.

at 1500°C and then exposed to oxygen at a pressure of 1.3×10^{-3} Pa at 1300°C. The oxygen pressure was monitored with a Veeco ionization gage. The specimens showed no weight loss and remained bright after 2000 hr of oxygen exposure. Metallographic examination revealed no indication of an oxide film on the surface or of oxygen penetration along the grain boundaries (Fig. 19*a* and *b*). The tensile properties of the exposed specimens were determined at five temperatures; the results are presented in Table 17. The exposure to oxygen at 1300°C did not impair the ductility of iridium and Ir-0.3% W at room or elevated temperatures. In fact, most of the exposed specimens exhibited a better ductility than the unexposed ones. The tensile strength was not sensitive to the oxygen exposure, although the yield strength of the exposed specimens is a little lower than that of the unexposed ones. Thus, exposure to the low-pressure oxygen at 1300°C does not have a detrimental effect on the tensile properties of iridium and Ir-0.3% W.

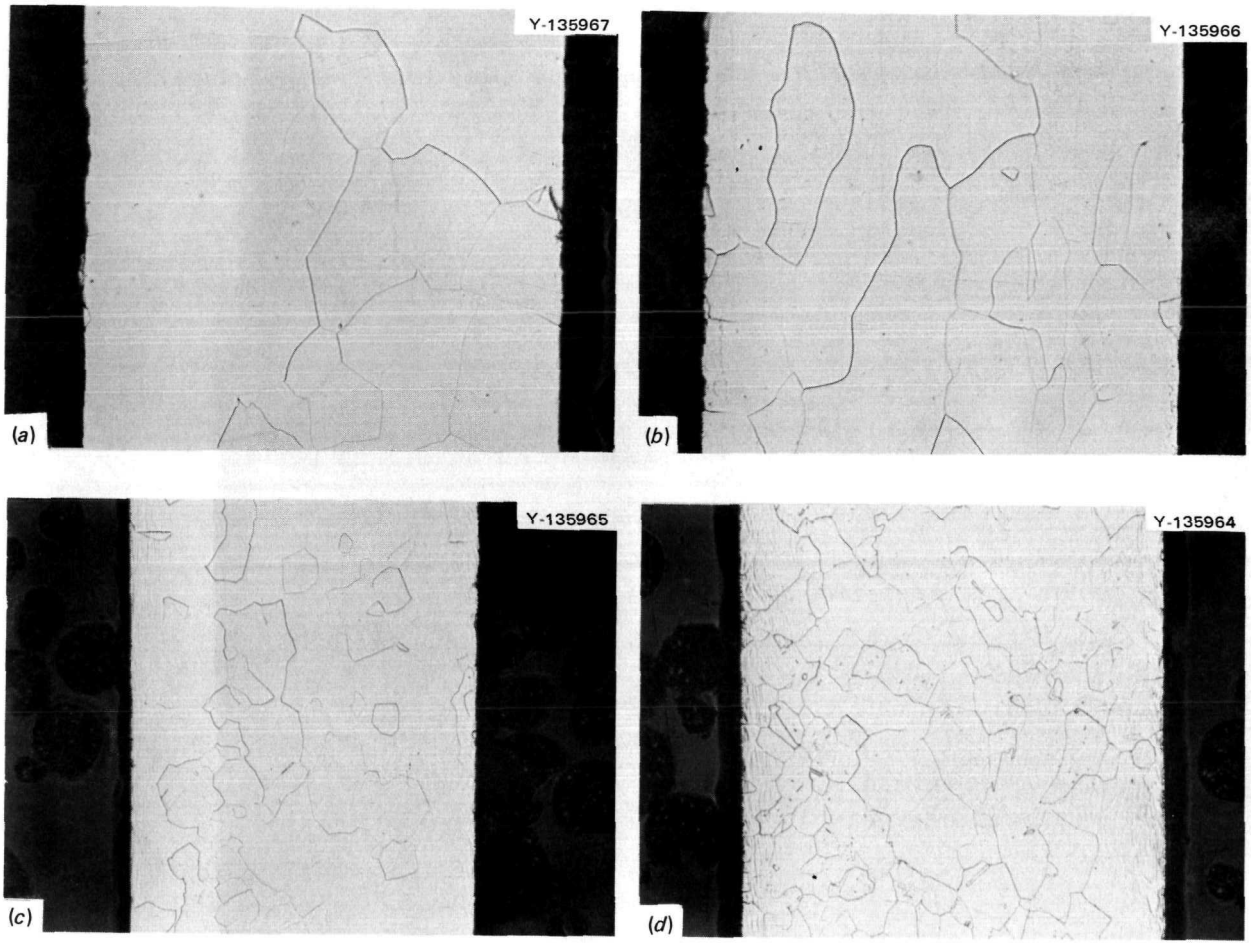

Fig. 19. Microstructures of (*a*) Iridium (S-65) and (*b*) Ir-0.3% W (S-74) exposed to oxygen at 1.3 x 10^{-3} Pa for 1000 hr at 1300°C, (*c*) Ir-1.92% W (Ir-15) and (*d*) Ir-3.84% W (Ir-29) exposed to oxygen and carbon at a total pressure of 1.3 x 10^{-3} Pa for 1000 hr at 1300°C; 100×.

Table 17. Tensile properties[a] of iridium and Ir-0.3% W sheet specimens[b] exposed to 1 x 10^{-3} Pa O_2 at 1300°C

Alloy (wt %)	Exposure time (hr)	Strength (ksi)[c]		Elongation (%)
		Yield	Tensile	
		Room temperature		
Ir	0	17.0	57.0	9.5
Ir	1000	9.5	54.3	9.3
Ir	2000	13.0	54.5	9.7
		500°C		
Ir	0	14.5	64.0	13.5
Ir	1000			
Ir	2000	11.0	67.0	16.5
		760°C		
Ir	0	18.0	52.0	21.5
Ir	1000	10.0	59.0	24.2
Ir	2000	13.5	60.7	25.7
Ir-0.3 W	0	16.0	60.5	25.0
Ir-0.3 W	1000	12.0	63.5	28.2
		1090°C		
Ir	0	15.0	32.3	37.8
Ir	1000	13.5	31.0	32.2
Ir	2000	11.6	31.6	37.3
		1316°C		
Ir	0	6.0	23.0	37.5
Ir	1000	6.8	22.5	34.0
Ir	2000	6.5	23.5	43.7

[a] Tested at 0.05 to 0.1 in./min strain rate.

[b] Recrystallized 1 hr at 1500°C.

[c] 1 ksi = 6.89 MPa.

To simulate the MHW heat source environment, tensile specimens of Ir-1.92% W and Ir-3.84% W alloys heat treated for 1 hr at 1500°C were contacted with ATJ graphite on one side and exposed to oxygen on the other side at a total pressure of 1.3 x 10^{-3} Pa at 1300°C. Figure 20 shows the arrangement of the specimens in the ATJ graphite boat. Both sides of the specimens were bright and showed no indication of surface reaction with oxygen or carbon after the 1000-hr exposure. Weight measurement also revealed no change in weight after the exposure. The

Y 126379

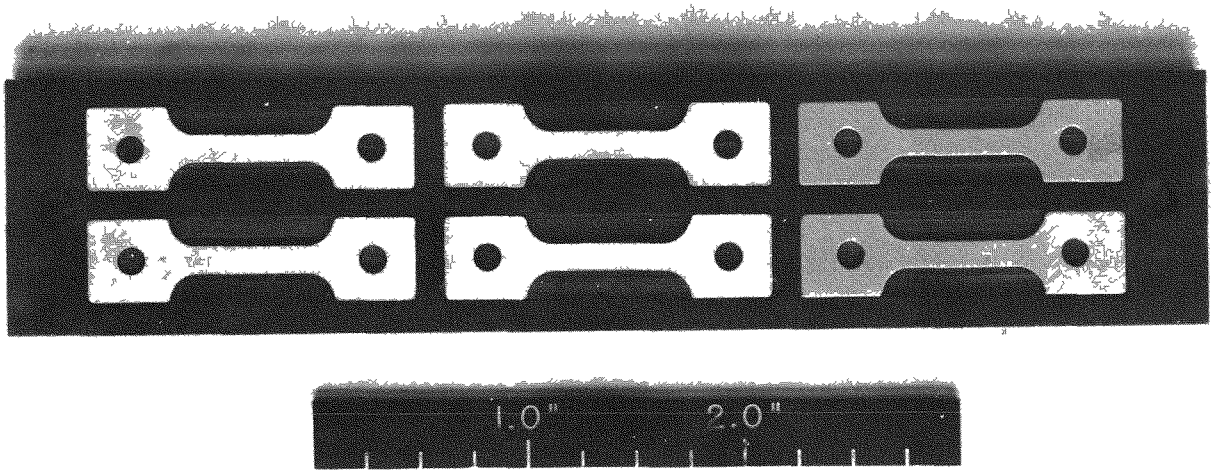

Fig. 20. Arrangement of iridium-tungsten test specimens in the ATJ graphite boat.

photographs in Fig. 19*c* and *d* show no indication of internal oxidation or oxygen penetration along the grain boundary. The results of tensile tests are compared in Table 18 with those for the unexposed specimens. The tensile strength is not sensitive to the exposure, whereas the yield strength of the exposed specimens is a little lower than for the unexposed ones. As indicated in Table 18, the exposure to an oxygen and graphite environment at 1300°C does not impair the ductility of the iridium-tungsten alloys at the test temperatures.

The interstitial content of both the specimens exposed to oxygen and those exposed to carbon and oxygen was determined by vacuum fusion analysis; the data are presented in Table 19. The carbon and oxygen concentrations decreased in both environments, suggesting that their concentration in the fabricated specimens may be higher than the concentration in equilibrium with these environments. The data in Table 19 indicate that the solubility of carbon in the iridium-tungsten alloys may be less than 10 ppm and the solubility of oxygen less than 5 ppm; these values are in good agreement with the results obtained from the air oxidation study (see Table 15). There was no change in concentration of nitrogen and hydrogen during the exposures.

Table 18. Tensile properties[a] of iridium-tungsten sheet specimens[b] contacted with ATJ graphite on one side and exposed to oxygen at a total pressure of 1 x 10^{-3} Pa at 1300°C

Alloy (wt %)	Exposure time (hr)	Strength (ksi)[c] Yield	Strength (ksi)[c] Tensile	Elongation (%)
		Room temperature		
Ir-1.92 W	0[d]	36.7	70.3	8.3
	1000	33.7	68.2	7.9
Ir-3.84 W	0[d]	51.7	64.0	4.0
	1000	46.8	62.5	3.8
		760°C		
Ir-1.92 W	0[d]	22.2	84.2	30.0
	1000	19.6	85.0	28.3
Ir-3.84 W	0[d]	30.0	57.3	10.6
	1000	30.1	88.2	19.8
		1093°C		
Ir-1.92 W	0[d]	22.2	60.5	31.2
	1000	17.8	60.8	41.4
		1316°C		
Ir-1.92 W	0[d]	17.0	45.2	36.0
	1000	16.0	47.1	37.0
		1370°C		
Ir-3.84 W	0[d]	21.7	46.9	25.1
	1000	22.2	44.0	27.3

[a]Tested in vacuum at a crosshead speed of 0.05 to 0.1 in./min.

[b]All specimens were annealed for 1 hr at 1500°C prior to exposure to graphite and oxygen.

[c]1 ksi = 6.89 MPa.

[d]Unexposed specimens were vacuum annealed for 1 hr at 1500°C prior to tensile testing.

Table 19. Interstitial content[a] in iridium-tungsten sheet specimens[b] exposed to oxygen or oxygen and carbon at 1300°C and at 1 x 10^{-3} Pa pressure

Exposure condition		Interstitial content (ppm)			
Environment	Time (hr)	Oxygen	Hydrogen	Nitrogen	Carbon
		Ir (S-65)			
Oxygen	0	9	1	1	5
	1000	5	1	1	6
	2000	1	1	1	5
		Ir-0.3% W (S-74)			
Oxygen	0	10	1	1	5
	1000	8	1	1	1
		Ir-1.92% W (Ir-15)			
Oxygen and carbon	0	8	1	1	11
	1000	3	1	1	10
		Ir-3.84% W (Ir-29)			
Oxygen and carbon	0	2	1	1	18
	1000	1	1	4	8

[a]Obtained from vacuum fusion analysis.

[b]Annealed 1 hr at 1500°C prior to exposure.

GENERAL DISCUSSION, SUMMARY, AND FUTURE WORK

Impurity Effects

The physical and mechanical properties of iridium and iridium-tungsten alloys are quite sensitive to trace impurities in the ppm range. The fracture behavior, yield strength, and recrystallization behavior are particularly sensitive to impurities, as discussed below.

Fracture Behavior

Examination of the tensile fracture behavior reveals that the iridium and iridium-tungsten sheets produced from the EI material are more resistant to grain-boundary separation than the sheets produced

from the OEP or MB powders. The EI material contains higher levels of trace impurity, as shown in Table 1. This suggests that some impurities in the EI material play an important role in strengthening the grain-boundary region and in suppressing the brittle grain-boundary fracture. To identify such impurities, the fracture surfaces of the EI and OEP tensile specimens broken at room temperature were analyzed by the SSMS analysis. The results are presented in Table 20 for bulk concentration (corresponding to long-time exposure of fracture surface to the spark source) and for surface concentration (corresponding to shorter time exposures). Because the specimens fractured mainly by GBS at room temperature, the surface concentration in Table 20 may be considered as the impurity level in the vicinity of the grain-boundary regions. The range of concentrations between the surface and under surface regions may also be interpreted as the impurity gradient near the grain boundary. The trace impurity level in the EI material is much higher than that in the OEP sheets, as confirmed in Table 20. Auger work[17] at ORNL indicates that carbon and oxygen are not strongly segregated on grain boundaries and that their concentration is also not significantly different in the EI and OEP materials. All of this suggests that the grain boundary in iridium is intrinsically weak and that the GBS is alleviated rather than caused by the segregation of impurities on grain boundaries.

The impurity elements whose concentration is significantly higher in the EI than in OEP materials are listed in Table 21. The impurities fall into two categories — elements such as thorium, tantalum, iron, and aluminum, whose concentration at the grain boundary is higher than the bulk value by two to four orders of magnitude, and second, elements such as rhodium and nickel, whose grain-boundary concentration is not significantly different from bulk value. Thus, we suspect that the elements with distinctly higher grain-boundary concentrations contribute to the major difference in fracture behavior of EI and OEP materials. Future work will involve the preparation of iridium-tungsten alloys doped with these elements to study the effect of dopants on the fracture behavior at various test conditions.

Yield Behavior

The critical resolved shear stress of an iridium single crystal has been reported[18,19] to be exceptionally high as compared with that of other fcc metals; however, the present work indicates that the yield strength of high-purity iridium polycrystals is not inordinately high. Figure 8*a* indicates that the σ_y of iridium is very sensitive to the trace impurity. The electron-beam-melted iridium produced from OEP and MB powders (ORNL material) has a low σ_y of 55.1 to 68.9 MPa, whereas the EI iridium containing higher levels of impurity has a yield strength of 172.3 MPa at room temperature. Mehan et al.[20] have reported that the σ_y of impure iridium can be as high as 261.8 MPa at room temperature. The yield strength of the ORNL iridium (EBP-21, EB) is not dependent on the test temperature even up to 1100°C, as shown in Fig. 8*a*. This strongly indicates the absence of short-range stress fields, which

Table 20. Chemical analysis[a] of iridium and iridium alloy sheet specimens[b] fractured at room temperature

Element	S-74[c]		EI-52[f]		EI-114[g]		EBP-21[h]		WC-4[i]		WD-1[i]		WE-3[i]		Ir-1.92% W[i]	
	Bulk[d]	GB[e]	Bulk[d]	GB[e]	Bulk[d]	GB[e]	Bulk[d]	GB[e]	Bulk[d]	GB[e]	Bulk[d]	GB[e]	Bulk[d]	GB[e]	Bulk[d]	GB[e]
Al	70	10-70	20	50-1000	60	1000-10,000	1	50-200	2	50-150	0.1	10-30	1	20	1	20-80
B	1.4	30	0.2	<10	0.2	20-70	0.2	5-20	0.2	10	<0.2	<10-30	0.2	5-10	0.2	5-20
Ca	30	50-200	6	20-100	2	200-800	6	30-200	6	10-30	0.2	10-100	1	20-100	6	50
Co	2		11		0.3		0.3		6		<0.1		0.1		6	
Cr	100	<20	10	100-2000	3	300-1500	3	50-200	30	<20	1	<50-200	0.5	20-100	3	<20-50
Cu	30	20	30	100-300	50	100-400	10	<20-200	3	<20	5	<20	2	30-100	3	<20
Fe	400	200-600	150	100-4000	15	1000-3000	15	200-2000			3		2			
Hf			<0.4		<0.4		<0.4		<0.4						<0.4	
K	0.6	30-70	0.6	20-150	2	800-8000	2	100-1000	6	50-200	<0.2	10-500	<0.2	100-400	6	50-250
Mg	5		0.4		0.4		0.4		0.4		<1		<1		<0.4	
Mn	3		3		1		0.3		0.3		<0.3		<0.3		0.3	
Mo	3		3		1		3		3		3		<3		10	<50-100
Ni	50	<50	10	20-200	10	20-50	1	<50	1	<20	1	<20	1	<50	1	<20
Os			<0.4		<0.4		<0.4		<0.4						<0.4	
P	0.3		0.2		<0.1		<0.1		0.3		<0.2		<0.2		0.1	
Pd	20		6		0.6		<0.2		0.2		5		1		<0.2	
Pt	100		1		1		1		1		2		<1		1	
Re	0.5	<0.5	<0.2		<0.2		<0.2		<0.2		0.2		0.2		6	
Rh	150		50		50		20		2		2		10		2	
Ru	150		2		0.5		20		20		20		1		20	
Si	60	50-90	3	100-500	10	500-2000	10	200-1000	100	200-600	9	50-1000	15	200	30	200-600
Sn			6		0.6		<0.2		<0.2		<0.2				<0.2	
Ta	10	<50	30	80-3000	3	2000-5000	3	<100	3	<50	3	20-300	<3	<50	3	<100
Th	10	1000-10,000	10	2000-20,000	1	<50-5000	<0.1	<50-800	<0.1	<100	<0.1	<50		<50	<0.1	<100
Ti	5		1	50	1	100-600	1	<50	⩽3		2		1		⩽3	<50
V	3		3		1	<10-50	3		3		<1				3	
W	3000	4000	4000	∿4000	∿1%		10	<1000	4000	4000-15,000	3000	3000	3000	3500	<1%	∿2%
Zn		<20	0.1	<50-300	0.1	100-600	0.1	<20	0.1	<20	<1	<20	<1	20	<0.1	<20
Zr	1		0.3		0.1		0.1		0.3						1	
Br			0.3	50-500	<0.1		0.1		<0.1						<0.1	
S	7	<50-200		50-300	1	800-8000	3	600-3000	1	<50	<2	<50-500	<2	<50-400	1	<50-1000
Cl		100-300		50-300		1000-10,000		200-1000		<50-200		50-1000		100-500		200-600

[a] Analysis in parts per million by SSMS method.

[b] Annealed for 1 hr at 1500°C prior to tensile testing.

[c] Engelhard Industries 1/8-in. plate fabricated to sheet at ORNL.

[d] Bulk concentration obtained from long-time exposure of fracture surface to ionized beam.

[e] Grain boundary. Surface concentration obtained from various short-time exposures of fracture surface to ionized beam.

[f] PICS produced from EI material, lot No. 52.

[g] Sheet produced by EI.

[h] Iridium produced from OEP powder.

[i] Ir-3% W produced from OEP powder.

Table 21. The difference in trace impurity[a] observed in OEP and EI sheets

Element	EI sheet		OEP sheet	
	Grain boundary	Bulk	Grain boundary	Bulk
Th	1,000-13,000	6	<50-150	<0.1
Ta	1,050-4,000	17	20-120	3
Al	500-6,000	40	30-100	2
Fe	500-3,500	85	80-750	15
Ni	20-130	10	<30	1
Rh		50		11

[a]In parts per million by weight.

generally contribute[21] to the thermally activated component of the yield strength. In other words, this suggests that the ORNL iridium is very pure and free from the hardening due to impurity solute atoms. In contrast, the yield strength of the EI iridium sheets containing high levels of trace impurities shows a temperature dependence, and its value decreases with test temperature, as shown in Fig. 8*a* and as reported by Mehan et al.[20] The yield strength of iridium-tungsten alloys increases with tungsten content, indicating the solution headening of iridium by tungsten. The degree of solution hardening by tungsten is strongly temperature-dependent, and the yield strength decreases with test temperature, as shown in Fig. 13.

Recrystallization Behavior

The recrystallization behavior of iridium and Ir-0.3% W alloys has been found to be very sensitive to trace impurities in the ppm range. Recrystallization of the iridium sheet EBP-21 produced from the OEP powder starts at 800°C and is complete at 950°C. These recrystallization temperatures agree with the data reported for iridium in literature.[22,23] The recrystallization behavior of Ir-0.3% W sheets used for hardware production has been studied[4,24] extensively, and the results indicate a lot-to-lot variation in the range of 100°C for the OEP sheets. The iridium sheets produced from the MB powder had higher recrystallization temperature. For instance, the 100% recrystallization temperature of EB sheets is found[6] to be 1175°C based on the recrystallization study at Mound Laboratories. Because the EI sheets contain a relatively high level of trace impurities, their recrystallization temperature is distinctly higher than that of the OEP sheets. We characterized the recrystallization behavior of the EI sheet S-69 and found its recrystallization temperature to be higher than that of the OEP sheets by as much as 400°C. Some PICS produced from the EI material even showed a duplex structure after annealing at 1300°C, as indicated in Fig. 7*a*. This structure is believed to have resulted from a surface contamination that raises the recrystallization temperature of the material near the surface.

Tungsten Effects

Alloying with up to 4% W significantly affects the physical and mechanical properties of iridium. As shown in Fig. 6, the recrystallization temperature of iridium increases with the tungsten content. Increasing the recrystallization temperature is required in iridium for controlling the metallurgical structure of sheets during hot working. Alloying with tungsten also inhibits the grain growth, as shown in Table 3. Refinement of grain structure is generally beneficial to the mechanical properties, such as impact properties.[25]

The iridium-tungsten alloys have good oxidation resistance below 1000°C (Table 14). The Ir-1.92% W has the lowest oxidation rate among the alloys at 770 and 870°C. The air oxidation rate of iridium-tungsten alloys is higher than that of platinum-30% rhodium-8% tungsten alloy (Pt-3008)[26] by more than two orders of magnitude at 1000°C; however, at 770°C, their rate is even lower than that of Pt-3008 by an order of magnitude. In addition, the iridium-tungsten alloys containing 2% tungsten showed no indication of internal oxidation and grain-boundary penetration (Figs. 16-18) between 770 and 1000°C. Thus, Ir-1.92% W alloy has the excellent oxidation resistance to withstand the postimpact oxidation of MHW PICS.

The strength of iridium-tungsten alloys increases with the tungsten content. The linear increase in yield strength with tungsten concentration in Fig. 13 is in agreement with the solution hardening theory predicted by Mott and Nabarro.[27] The ductility of iridium-tungsten alloys generally decreases with the tungsten content; however, the elongation at 1370°C is independent of tungsten content up to 2%. Among the alloys, Ir-2% W exhibits the highest combination of strength and ductility at 1370°C, and thus has the highest toughness at this temperature. In fact, the toughness of Ir-1.92% W is significantly greater than that of potential fuel-clad materials such as Pt-3008, TZM, and T-111 at 1300 to 1400°C.

In addition to the excellent tensile properties, the Ir-1.92% W alloy appears to be compatible with graphite and the simulated heat source environments. This alloy is readily fabricated into sheet and presents no major difficulties when formed from sheet into hemispheres or cylindrical capsules. Therefore, our study leads to the conclusion that the optimum amount of tungsten in iridium should be around 2%.

Strain Rate Effects

As indicated in Table 10, the Ir-0.3% W alloy is very ductile when tested at slow strain rates (10^{-4} m/sec) above 1000°C. In this temperature range, the alloy actually had more than 50% tensile elongation and fractured by ductile rupture with close to 100% reduction in area. However, on impact of MHW fuel sphere assemblies at a velocity of about 90 m/sec, the Ir-0.3% W PICS quite often showed brittle failure with limited deformation even at 1400°C. Two types of failure are generally observed[3,25,28] on the impacted shells: one is a tensile failure in the hoop strain region, where the normal strain is maximum (6 to 15%);

the other one is the so-called fingerprint crack on the impact face, where fine cracks are formed within an annular region, with no cracks in the rest of the impact face. An Ir-1.92% W fuel sphere assembly (MHT-74) impacted at General Electric at 90 m/sec and at 1427°C showed[29] fingerprint cracks on the impact face with only limited deformation. Thus, alloying with tungsten does not inhibit brittle fracture of iridium when impacted at high velocities (90 m/sec or higher).

Comparison of the tensile with the impact results shows that the ductility and fracture behavior of iridium and iridium-tungsten alloys are sensitive to the test velocity. Tensile tests at intermediate strain rates have been performed[30] at Donald W. Douglas Laboratories, and the results show that Ir-0.3% W and Ir-1.92% W alloys remain ductile at a test velocity of 3 to 5 m/sec at 1370°C. Tensile tests at strain rates close to the MHW impact velocity (90 m/sec) are currently being conducted at ORNL to verify the strain rate effects.

Postmortem examination of iridium-tungsten PICS revealed[3,25,28,30] that the failures occurred mainly by GBS when impacted at 90 m/sec at 1400°C. The same fracture mode was observed when tested at low temperatures and strain rates (Figs. 9 and 12). Auger[17] and SSMS analyses indicate no major segregation of impurities on grain boundaries, suggesting that the grain boundary is intrinsically weak in iridium and in iridium-tungsten alloys. We have found that the trace impurities listed in Table 21 tend to segregate on grain boundaries and improve the fracture behavior. In an attempt to develop a more impact resistant alloy, the elements listed in Table 21 will be added to the iridium-tungsten alloys in order to study their effects on the fracture behavior and impact properties.

ACKNOWLEDGMENTS

The authors are grateful to R. G. Donnelly and A. C. Schaffhauser for their significant contribution to managing the program. Thanks are extended to J. N. Newsome for technical assistance; D. E. Harasyn, D. N. Braski, G. A. Reimann, G. E. Angel, J. N. Hix, and G. D. Goldston for alloy preparation and fabrication; C. L. White for Auger analysis; J. C. Franklin and R. Sites for SSMS; J. I. Federer for iridium powder preparation; W. H. Farmer for metallography; and T. J. Henson for scanning electron microscopy. We thank J. H. DeVan, W. R. Martin, and C. L. White for reviewing the technical content of this manuscript and the Technical Publications Department, Information Division, for preparing the manuscript for publication.

REFERENCES

1. C. T. Liu, H. Inouye, and R. W. Carpenter, *Metall. Trans.* 4(8): 1839-50 (1973).

2. H. Inouye and C. T. Liu, *Low-Pressure Oxidation of T-111 and Effect on Tensile Properties*, ORNL/TM-4621 (August 1974).

3. General Electric Company, *Multi-Hundred Watt Radioisotope Thermoelectric Generator Program, Parts I and II, Annual Report 1 January 1973-31 December 1973*, GESP-7107 and GEMS-418.

4. D. N. Braski and A. C. Schaffhauser, *Production of Ir-0.3% W Disks and Foil*, ORNL/TM-4865 (April 1975).

5. R. G. Frank, A. C. Schaffhauser, and W. G. Wyder, *Backup Ir Hemisphere Program Task Force Report*, Report GESP-744 (April 1974).

6. W. C. Wyder, Monsanto Research Corporation, private communication, 1974.

7. E. J. Rapperport and M. F. Smith, Technical Report WADD-TR-60-132, Part II (AD 287548) (1962).

8. Mound Laboratories, quality control samples data sheet presented in the meeting held at ORNL in September 1974.

9. P. W. Bridgman, *Trans. Am. Soc. Met.* 32: 612 (1960).

10. M. A. Fortes and B. Ralph, *Acta Metall.* 15: 707 (1967).

11. Paul W. Palmberg, letter to R. L. Mehan, December 9, 1971.

12. E. H. P. Cordfunke and G. Meyer, *Rec. Trav. Chim.* 81: 495 (1962).

13. E. H. P. Cordfunke and G. Meyer, *Rec. Trav. Chim.* 81: 670 (1962).

14. W. L. Phillips, *ASM Trans. Q.* 57: 33-37 (1964).

15. J. M. Crisione et al., Technical Report, ML-TDR-64-173, Part II (AD 608092) (1964).

16. M. R. Naadler et al., *J. Phys. Chem.* 64: 1468-71 (1960).

17. C. L. White, ORNL, private communication, June 1975.

18. C. A. Brookes, J. H. Greenwood, and J. L. Routbort, *J. Inst. Met.* 98: 27 (1970).

19. R. W. Douglas et al., *High-Temperature Properties and Alloying Behavior of the Refractory Pt-Group Metals*, NP-10939, Battelle Memorial Institute (1961).

20. R. L. Mehan, E. D. Duderstart, and E. H. Sayell, *Metall. Trans.* 7A: 885 (1975).

21. R. J. Arsenault, "Low Temperature of Deformation of bcc Metals and Their Solid Solution Alloys," in *Treatise on Materials Science and Technology*, vol. 6, *Plastic Deformation of Metals*, ed. by R. J. Arsenault, Academic Press, New York, 1975, pp. 1-95.

22. W. Betteridge, "The Consolidation Working and Properties of Ir and Ru," pp. 525-51 in *Metalle für die Raumfahrt* (Proc. 5th Plansee Seminar, Reutte, Tirol, Austria), ed. by F. Benesonsky, Metallverk Plansee AG, Reutte, Tirol, Austria, 1965.

23. British Patents No. 1,051,224; 1,016,809.

24. D. E. Harasyn, ORNL, private communication, October 1975.

25. S. S. Hecker, LASL, private communication, November 1975.

26. H. Inouye, C. T. Liu, and R. G. Donnelly, *New Pt-Rh-W Alloys for Space Isotopic Heat Sources*, ORNL-4813 (September 1972).

27. N. F. Mott and F. R. N. Nabarro, *Proc. Phys. Soc.* 52: 86 (1940).

28. E. H. Sayell, General Electric Company, private communication, 1974-1975.

29. C. T. Liu and H. Inouye, *Postmortem Analysis of Ir-2% W Postimpact Containment Shell*, ORNL/TM-4943 (July 1975).

30. J. D. Wattrous and D. E. Knapp, Donald W. Douglas Laboratories, McDonnell Douglas Astronautic Company, Richland, Washington, private communication, April and May 1974.

Blank page

ORNL-5240
Distribution
Category UC-25

INTERNAL DISTRIBUTION

1. D. N. Braski
2. C. R. Brinkman
3. J. A. Carter
4. F. L. Culler
5. J. E. Cunningham
6. J. H. DeVan
7. J. R. DiStefano
8. R. G. Donnelly
9. J. I. Federer
10. G. M. Goodwin
11. J. P. Hammond
12. D. E. Harasyn
13. R. L. Heestand
14. R. F. Hibbs
15-17. M. R. Hill
18-22. H. Inouye
23. J. R. Keiser
24. E. Lamb
25-29. C. T. Liu
30. M. M. Martin
31. W. R. Martin
32. R. E. McDonald
33. C. L. Ottinger
34. H. Postma
35-36. A. C. Schaffhauser
37. G. M. Slaughter
38. J. O. Stiegler
39. V. J. Tennery
40. D. B. Trauger
41. J. R. Weir, Jr.
42. C. L. White
43. R. O. Williams
44-45. Central Research Library
46. Document Reference Section
47-56. Laboratory Records
57. Laboratory Records, ORNL RC
58. ORNL Patent Office
59. P. M. Brister (Consultant)
60. John Motiff (Consultant)
61. Hayne Palmour III (Consultant)
62. J. W. Prados (Consultant)
63. N. E. Promisel (Consultant)
64. D. F. Stein (Consultant)

EXTERNAL DISTRIBUTION

65. AiResearch Manufacturing Company of Arizonia, 402 South 36th Street, P.O. Box 5217, Phoenix, AZ 85010
    J. E. McCormick
66. Battelle Memorial Institute, 505 King Avenue, Columbus, OH 43201
    C. Alexander
67. Fairchild Space and Electronics Company, Germantown, MD 20767
    A. Schock
68. General Electric Company, Materials Technology, Energy Systems Programs, 1 River Road, Schenectady, NY 12345
    R. G. Frank
69. General Electric Company, Nuclear Programs, P.O. Box 8661, Philadelphia, PA 19101
    E. W. Williams
70. Gulf Energy and Environmental Systems, P.O. Box 608, San Diego, CA 92112
    N. Elsner
71. Kirtland Air Force Base, NM 87117
    Directorate of Nuclear Safety

72-73. Los Alamos Scientific Laboratory, P.O. Box 1663, Los Alamos, NM 87545
S. E. Bronisz
S. Hecker

74. Minnesota Mining and Manufacturing Company, 2501 Hudson Road, St. Paul, MN 55119
E. F. Hampl

75. Monsanto Research Corporation, P.O. Box 32, Miamisburg, OH 45342
E. W. Johnson

76. Sunstrand Energy Systems, 4747 Harrison Avenue, Rockford, IL 61101
E. Kreuger

77-78. Teledyne Energy Systems, 110 W. Timonium Road, Timonium, MD 21093
W. J. Barnett
W. Osmeyer

79-89. ERDA Division of Nuclear Research and Applications, Washington, DC 20545
R. T. Carpenter
T. J. Dobry
W. D. Kenney
A. P. Litman
J. J. Lombardo
A. L. Mowery
G. A. Newby
B. J. Rock
C. O. Tarr
N. R. Thielke
E. J. Wahlquist

90. ERDA Oak Ridge Operations Office, P.O. Box E, Oak Ridge, TN 37830
Research and Technical Support Division

91-313. Technical Information Center, P.O. Box 62, Oak Ridge, TN 37830
In distribution as shown in TID-4500 Distribution Category UC-25 (25 copies to NTIS)

☆ U.S. GOVERNMENT PRINTING OFFICE: 1976-748-189/91